STRUCTURAL STUDIES OF CuV_2O_6 AND $Ca_2V_2O_7$

TO MY AUNT

STRUCTURAL STUDIES OF CuV_2O_6 AND $Ca_2V_2O_7$

by

DAN E. MANOLESCU-, B.Sc.

A Thesis

Submitted to the Faculty of Graduate Studies

in Partial Fulfilment of the Requirements

for the Degree

Master of Science

McMaster University

April 1974

MASTER OF SCIENCE (1974) McMASTER UNIVERSITY
(Metallurgy and Materials Science) Hamilton, Ontario

TITLE: Structural Studies of CuV_2O_6 and $Ca_2V_2O_7$

AUTHOR: Dan E. Manolescu, B.Sc.

SUPERVISOR: Professor C. Calvo

NUMBER OF PAGES: vi, 71

SCOPE AND CONTENTS:

The crystal structure of $Cu_2V_2O_6$ has been studied by X-ray diffraction techniques. CuV_2O_6 has been found to have a structure closely related to the mineral brannerite as do the majority of the metavanadates, but with lower symmetry. The refinement of the structure showed a bonding geometry consistent with the bond strength-bond length correlations for oxides which have been applied to other vanadate structures.

The symmetry and unit cell parameters of $Ca_2V_2O_7$ have been determined. The attempted solutions are described and suggestions are made for future work on this structure.

ACKNOWLEDGMENT

My sincere thanks and gratitude to my supervisor, Professor C. Calvo, for his patience and encouragement, valuable discussions and assistance throughout this research.

My thanks to Dr. H. D. Grundy and Dr. M. Krishnamachari for many helpful suggestions and stimulating discussions.

Many thanks are also due to Mr. R. Faggiani for his help during parts of this work and to all members of the Crystallography Group for their help in so many different ways.

Many of the faculty and postdoctoral fellows of the Department of Metallurgy and Materials Science have been very kind in their suggestions and discussions with me. To them, I remain deeply indebted.

I thank Mrs. H. Kennelly who has been an extremely cheerful and efficient typist.

Lastly, I gratefully acknowledge the receipt of financial support from McMaster University and the Department of Metallurgy and Materials Science in the form of a graduate assistantship.

Finally, my thanks to my wife Angela for her constant support, assistance and sacrifices through the long years of graduate study. Without her encouragement and practical aid, especially in the last few months, this work would never have reached a successful conclusion.

TABLE OF CONTENTS

INDEX OF TABLES

INDEX OF ILLUSTRATION

CHAPTER I

INTRODUCTION - REVIEW OF MV_2O_6 AND $M_2V_2O_7$ COMPOUNDS

Phosphates, arsenates and vanadates form chemically similar compounds. The latter two often crystallize in isotypic structures. Examples are such compounds as $nMO \cdot X_2O_5$ which are designated as ortho (n=3), pyro or di (n=2) and meta (n=1). The tetrahedral anion persists throughout the phosphate series, whereas in the arsenates there is octahedral coordination for n=1 tetrahedral coordination for $2<n<5$ and a mixture of these for $n>5$.

Metavanadates

The vanadates, at the start of this research, were less well investigated but those compounds with n=1 indicated environments with five strong V-O bonds and one weak long bond.

A number of divalent metavanadates MV_2O_6 have been found to crystallize in the brannerite structure of $ThTi_2O_6$ (1). These include, Cd, Ca, Zn, α-Hg, Mg and Co metavanadates (2-5) crystallize in the monoclinic system with possible space group C2/m, C2 or Cm (see Table 1.1). Only the Cd and Hg metavanadates have been found to be dimorphous. CdV_2O_6 has two possible phases, the low temperature (α) and high temperature (β) phases respectively.

The structure of α-CdV_2O_6 is isotypic with that of CaV_2O_6 (monoclinic, space group C2/m) and differs from that of β in

Table 1-1

Unit Cell Parameters for Metavanadate Structures

Compound	Space Group	a(Å)	b(Å)	c(Å)	α(°)	β(°)	γ(°)	Reference
ZnV_2O_6	C2	9.242(8)	3.526(3)	6.574(6)		110°20'(15)		4
β-CdV_2O_6	C2/m	9.359(8)	3.568(5)	6.980(6)		112°00'(15)		2
α-HgV_2O_6	C2,Cm, C2/m	9.580(5)	3.644(3)	6.655(6)		107°13'(16)		4
β-HgV_2O_6	Pbca	14.43(1)	5.894(5)	4.925(5)				4
CoV_2O_6	C2/m	9.258(4)	3.505(1)	6.632(3)		111°65'(5)		8
MgV_2O_6	C2/m	9.279(7)	3.502(2)	6.731(6)		117°77'(6)		5
BaV_2O_6	C222	8.48	12.60	7.91				6
CuV_2O_6	$C\bar{1}$	9.168(5)	3.543(3)	6.478(7)	92.25(8)	110°34'(7)	91.88(6)	9

a breaking of the long sixth V-O interaction. This results in a contraction of the cell dimensions at high temperature. β-CdV_2O_6 has been refined by Bouloux and Galy (2) in space group C2/m while the structure of ZnV_2O_6 has been refined in space group C2 (4).

The high temperature phase β-HgV_2O_6 has a different structure. This phase crystallizes in an orthorhombic system with space group Pbca (4). In this structure the mercury and oxygen atoms form octahedra, while the vanadium atom is associated with an environment of five oxygen atoms. The structure consists of chains of VO_5 trigonal bipyramids. These chains form V-O sheets parallel with bc plane and held together by mercury atoms. Due to the fact that the listed bond lengths are accurate only to two figures we feel that the results are not reliable.

S. Launay and J. Thoret (6) have recently solved the structure of barium metavanadate. The compound crystallizes in an orthorhombic system with space group C222. In the crystal structure, the V and O atoms form tetrahedra. Each tetrahedron is linked to two neighbouring tetrahedra by an O atom, so that independent $(VO_3)_n^{n-}$ chains are formed. Two types of Ba atoms (dodecacoordinated and decacordinated, respectively) are inserted between the chains to provide cohesion in the structure.

The structure of copper metavanadate has been reported by Lavaud and Galy (7). They found a monoclinic structure and they assigned the space group C2. However, our results

show that this metavanadate crystallizes in a triclinic system with $C\bar{1}$ space group when the unit cell parameters are chosen to nearly parallel those of Lavaud and Galy.

Pyrovanadates

The next class of vanadate structures are the divanadates or pyrovanadates whose general formula is $X_2Y_2O_7$.

Brown and Calvo (10) pointed out that the crystals of composition $X_2Y_2O_7$ in which the radius of the X ion is less than that of Ca^{2+} tend to crystallize in structures related to thortveitite while those with greater radii crystallize in dichromate type structure. Baglio and Dann (11) have attempted to predict the structure type of these compounds from a plot of radius of X ions, R_x, versus the radius of Y ions, R_y, for known structures. Such a plot is shown in Fig. 1.1. Those compounds with ionic radius of Y larger than 0.5 Å crystallize in atopite structure. Below this value of the ionic radius they form the thortveitite structure ($Sc_2Si_2O_7$), R_x less than 0.9 Å, while the rest crystallize as a dichromate type structure.

It has been found that the geometric configuration of the anion $Y_2O_7^{n-}$ varies considerably from one structure type to another. For the atopite type structures the coordination number of Y is six and for the thortveitite and dichromate type structures the coordination number of Y is four.

In the latter two structures the diortho ion is formed by sharing YO_4 tetrahedra and they only differ in the relative

Figure (1-1)

The plot of the radius of 'X' versus the radius of 'Y' in compounds of the formula $X_2Y_2O_7$. The three structure type regions have been indicated. The dotted line represents the division between thortveitite and dichromate structure type. Circled data points represent solved structures.

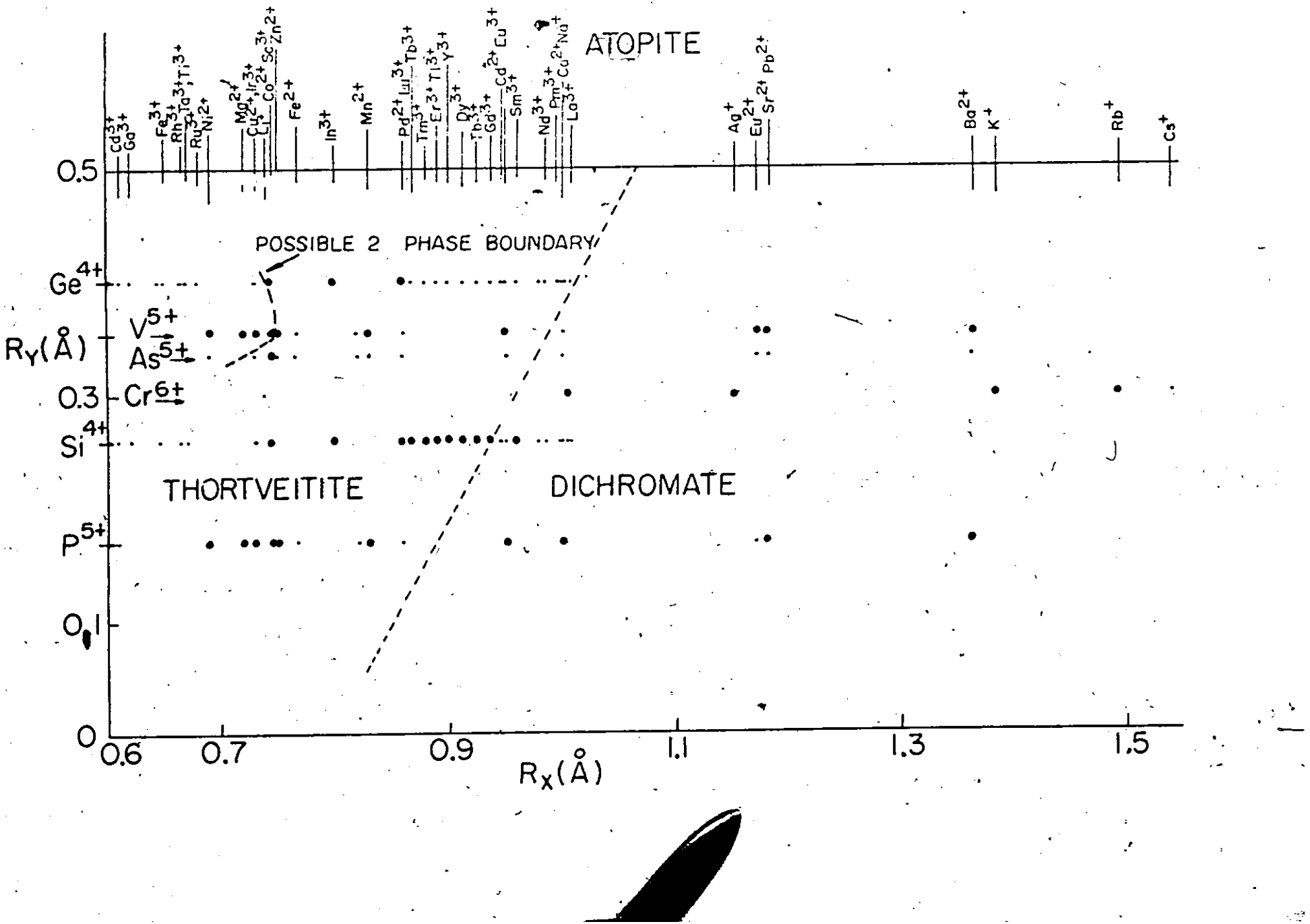
ATOPITE
POSSIBLE 2 PHASE BOUNDARY
THORTVEITITE
DICHROMATE
R_Y(Å)
R_X(Å)
0.5
0.3
0.1
0
0.6
0.7
0.9
1.1
1.3
1.5
Ge^{4+}
V^{5+}
As^{5+}
Cr^{6+}
Si^{4+}
P^{5+}
Cd^{3+} Ga^{3+} Fe^{3+} Rh^{3+} Ta^{3+} Ti^{3+} Ru^{3+} Ni^{2+} Mg^{2+} Cu^{2+} Ir^{3+} Li^{+} Co^{2+} Sc^{3+} Zn^{2+} Fe^{2+} In^{3+} Mn^{2+} Pd^{2+} Lu^{3+} Tb^{3+} Tm^{3+} Er^{3+} Tl^{3+} Y^{3+} Dy^{3+} Tb^{3+} Gd^{3+} Cd^{2+} Eu^{3+} Sm^{3+} Nd^{3+} Pm^{3+} Cu^{2+} Na^{+} La^{3+} Ag^{+} Eu^{2+} Sr^{2+} Pb^{2+} Ba^{2+} K^{+} Rb^{+} Cs^{+}

configuration of the $Y_2O_7^{n-}$ groups. In the thortveitite type structures, the oxygen atoms lie in a nearly staggered configuration while in the dichromate type they are in nearly eclipsed configuration. Divanadate members of the isotypes of thortveitite include $Mn_2V_2O_7$ (19), $Zn_2V_2O_7$ (12) and $Cd_2V_2O_7$ (20). There are many pyrophosphates which fall into this structure type and only a limited number of diarsenates. They usually undergo phase transitions where the high temperature forms are isomorphous with the mineral thortveitite and contain apparently linear X-O-Y bridging group, while the low temperature forms show a bent Y-$\hat{O}$-Y bond angle ranging from about 140°-156°. A similar transition is apparent in $Zn_2V_2O_7$ (12). The dichromate type includes many alkali dichromates and phosphates and the divanadates $Pb_2V_2O_7$ (13), β-$Sr_2V_2O_7$ (14) and $Ba_2V_2O_7$ (15).

In Table 1-2 a list of the unit cell parameters of all the reported structures of pyrovanadates are given. It can be seen from the table that many of the structures determined so far are either thortveitite (or dichromate) type or related to them; only a few are completely different. This suggests that the diagram from Figure 1-1 is only partially correct or that there is a transitional region. This possible phase region is indicated in Figure 1-1.

It is also to be noted that all rare-earth disilicates do fall quite close to the line dividing thortveitite and dichromate type structures. In the study of rare-earth disilicates, Felsche (16) reported the existence of five structural

Table 1-2

Unit Cell Parameters for Pyrovanadate Structures

Compound	a (Å)	b (Å)	c (Å)	α (°)	β (°)	γ (°)	Space Group	Structure Type	Ref.
$Mg_2V_2O_7$	13.767(7)	5.414(3)	4.912(2)	81.42(4)	106.82(4)	130.33(4)	$P\bar{1}$	Related to thortveitite	18
$Co_2V_2O_7$	6.594(2)	8.370(1)	8.470(9)		100.17(3)		$P2_1/c$	Distorted from $Mg_2V_2O_7$	18
$Ni_2V_2O_7$	6.515(8)	8.303(7)	9.350(6)		99.86(8)		$P2_1/c$		17
α-$Zn_2V_2O_7$	7.429(5)	8.340(3)	10.098(3)		111.37(5)		C2/c	Thortveitite	12
$Mn_2V_2O_7$	6.710(2)	8.726(2)	4.970(1)		103.57(1)		C2/m	Thortveitite	19
$Cd_2V_2O_7$	7.088(5)	9.091(5)	4.963(5)		103.21(5)		C2/m	Thortveitite	20
$Ca_2V_2O_7$	7.240(2)	6.663(2)	6.918(2)	96.35(2)	87.68(2)	119.55(2)	$P\bar{1}$	Unknown	Present work
β-$Sr_2V_2O_7$	7.055(2)	7.055(2)	25.64 (12)				$P4_1$	Dichromate	14
$Pb_2V_2O_7$	13.3689(7)	7.1607(4)	7.1027(4)		105.935(5)		$P2_1/a$	Dichromate	13
α-$Hg_2V_2O_7$	7.165(2)	3.636(1)	21.52 (4)				Pnma	Dichromate	22
$Ba_2V_2O_7$	13.571(6)	7.320(3)	7.306(3)	90.09(3)	99.48(4)	87.32(3)	$P\bar{1}$	Dichromate	15
$Cu_2V_2O_7$	20.645(20)	8.383(7)	6.442(12)				Fdd2	No relation	21

types. Some of these could be classified within thortveitite and dichromate structures. Since most of the structures belong to the thortveitite group, a brief description of this structure is appropriate.

The structure of thortveitite [$(Sc,Y)_2Si_2O_7$] consists of sheets of ScO_6 octahedra forming a hexagonal network on the ab plane, Fig. 1-2. Each ScO_6 octahedron shares three different edges with three separate ScO_6 octahedra forming infinite sheets interconnected by Si_2O_7 groups each of which share three oxygen atoms with two adjacent sheets. (Two of the terminal oxygen atoms are connected to one sheet while the third terminal oxygen atom is connected to the sheet above.) These sheets of metal ions are stacked along the c direction. All the structures isomorphous with thortveitite exhibit the same characteristics as thortveitite with however one long cation-oxygen bond per octahedron.

The structures of $Co_2V_2O_7$ and $Ni_2V_2O_7$ (17) and $Mg_2V_2O_7$ (18) are only partially related to thortveitite. The major difference between the structure of $Mg_2V_2O_7$ and thortveitite is in the linking of the anions in the former structure: one vanadium is coordinated to four oxygen atoms forming a slightly irregular tetrahedron while the second is five oxygen coordinated. The anions form chains composed of pairs of $V_2O_7^{4-}$ groups sharing edges across the centre of symmetry which run parallel to the c axis.

Figure (1-2)

A cation sheet in the structure of thortveitite. This shows the linking ScO_6 octahedra by shared edges.

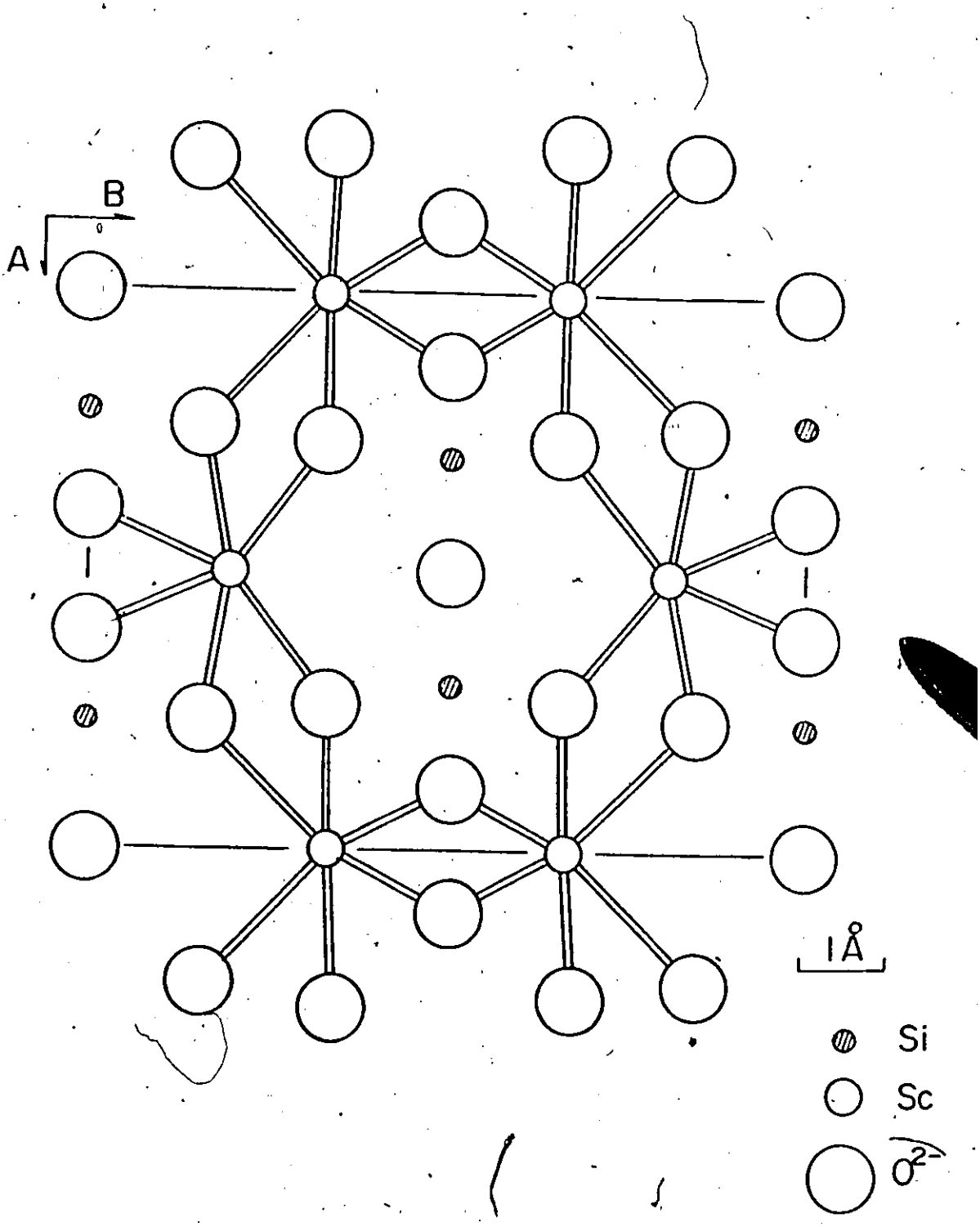
B
A
1Å
Si
Sc
O2-

In addition the hexagonal network of cation polyhedral chains found for thortveitite is lost as is the coplanarity of the Mg^{2+} ions which do not lie in the same plane; in addition half of the cations are bonded to the central bridging oxygen atom of the V_2O_7 groups.

As a result, one of the shared edges between MgO_6 octahedra is lost and replaced by a shared corner and thus the sheets of MgO_6 group are different than in thortveitite.

However, the oxygen atoms of the V_2O_7 groups are in a staggered configuration, a feature found in all thortveitite like structures. The structures of $Ni_2V_2O_7$ and $Co_2V_2O_7$ are also not related to thortveitite but more related to the previous one. Like in $Mg_2V_2O_7$ the hexagonal network of cations polyhedral chains is lost and half of the cations are bonded to the central bridging oxygen atom of the V_2O_7 group. Unlike the $Mg_2V_2O_7$ structure the anions $V_2O_7^{4-}$ are not linked together. On the other hand, the anion configuration is staggered in $Mg_2V_2O_7$ compared with nearly eclipsed configuration in $Co_2V_2O_7$ and $Ni_2V_2O_7$.

The structure of $Cu_2V_2O_7$ (21) differs from that reported for any divanadate with this stoichiometry. No correlation can be made with either dichromate or thortveitite type structures.

In this structure the $V_2O_7^{4-}$ ions have the staggered configuration and form sheets coincident with the bc plane. They also form chains parallel with the a axis. Adjacent sheets are generated by the diagonal glide plane and separated by a/4.

The Cu ions lie between V_2O_7 sheets and are coordinated strongly to four oxygen atoms (arising from four separate anions) and weakly to another one. The fifth oxygen atom is so bonded that CuO_5 and V_2O_7 groups in adjacent layers share an edge. The CuO_5 group in adjacent layers shares edges but all Cu-Cu bonds exceed 3 Å. The structure of $Ca_2V_2O_7$ is still unknown. An attempted solution will be described in Chapter III together with the single crystal data obtained.

However, from these examples a conclusion can be outlined. The attempt to predict the type of structures for the compounds of general compositions $X_2Y_2O_7$ after the plot presented in fig. 1-1 is far from correct, especially for the divanadate structures. The prediction that $Mg_2V_2O_7$, $Co_2V_2O_7$, $Cu_2V_2O_7$ would be a thortveitite like structure can be said to be wrong. It was suspected that the compounds which appear to the left of the proposed dotted line of the diagram 1-1, indicating a possible second phase boundary, will form a group of compounds similar in their deviation from the thortveitite structure. Like we have seen this doesn't seem to be true, especially in vanadium compounds. One explanation can be that the vanadium ion (V^{5+}) in oxide structures is found in environments with a variety of coordination numbers and distorts from regular polyhedron. The ease of the formation of this variety of coordination and distortion found might be due to the involvement of the empty 3d orbitals and also to the size of V^{5+} (= 0.54 Å) (e.g. As^{5+} with completely filled 3d orbitals, does

not show a variety of cordination but is mostly tetrahedral and rarely octahedral and has approximately the same size.)

CHAPTER II

THEORY

X-ray diffraction by a lattice

Crystals are composed of groups of atoms with the same orientation repeated at regular intervals in three dimensions. For certain purposes it is sufficient to regard each group of atoms as replaced by a representative point and the collection of points so formed is the space lattice or lattice of the crystal.

The lattice is important because it provides a basis for the theory of x-ray diffraction by the crystal: that is the angles of diffraction of the x-rays depend only upon the dimensions of the lattice. Let be an electron at $\vec{r}$

$$\vec{r} = n_1\vec{a} + n_2\vec{b} + n_3\vec{c} \qquad (2.1)$$

where $\vec{a}$, $\vec{b}$, $\vec{c}$ are the unit cell parameters and n_1, n_2 and n_3 are integers.

The path difference between two parallel waves scattered from two different electrons in the crystal lattice will be

$$\lambda\vec{r}\cdot\vec{S}$$

where λ is the wave length of the radiation, $\vec{r}$ is the vector distance between the scattering electrons, and $\vec{S}$ is the scattering vector which represents the difference between

the scattering vector $\vec{s}_1$ and incident vector $\vec{s}_0$:

$$\vec{S} = \vec{s}_1 - \vec{s}_0 \qquad (2.2)$$

$\vec{s}_1$ and $\vec{s}_0$ are unitary vectors of modulus $\frac{1}{\lambda}$.

In order that the waves be scattered in phase, this path difference should be equal to a whole number of waves and thus $\vec{r}\cdot\vec{S}$ must be equal to an integer:

$$(n_1\vec{a} + n_2\vec{b} + n_3\vec{c})\cdot\vec{S} = \text{integer}.$$

From this condition Laue's equations follow immediately:

$$\begin{aligned} \vec{a}\cdot\vec{S} &= h \\ \vec{b}\cdot\vec{S} &= k \\ \vec{c}\cdot\vec{S} &= \ell \end{aligned} \qquad (2.3)$$

where h, k, ℓ are integers.

Only when Laue's equations are simultaneously satisfied can a diffracted beam be produced.

We will consider now equation (2.2) in more detail. The magnitude of the right side is $|\vec{s}_1 - \vec{s}_0| = 2\sin\theta/\lambda$ where 2θ is the scattering angle. Now it can be shown very easily that the vector $\vec{S}$ is perpendicular to the hkℓ plane and its magnitude is equal to $1/d_{hk\ell}$ (23). The spacing d is the perpendicular distance of the plane hkℓ from the origin. Accordingly we have:

$$\frac{2\sin\theta}{\lambda} = \frac{1}{d}. \qquad (2.4)$$

This is the Bragg equation.

Reciprocal lattice

It is convenient to work on a coordinate system in which the solutions of the Laue's equations can be easily calculated. We have mentioned that each vector $\vec{S}$ of magnitude $\frac{1}{d_{hk\ell}}$ is perpendicular to the plane hkℓ. These vectors define a set of lattice points - the reciprocal lattice. (It can be seen immediately that the end points of these vectors satisfy the three Laue equations simultaneously because each point is found at the intersections of the three planes perpendicular to $\vec{a}$, $\vec{b}$ and $\vec{c}$ respectively.). The unit cell of this lattice is defined by three vectors, which are usually called $\vec{a}^*$, $\vec{b}^*$ and $\vec{c}^*$ and each point in this lattice is defined by three numbers, h, k and ℓ. These three non-coplanar vectors were defined by J. W. Gibbs as:

$$\vec{a}^* = \frac{\vec{b}\times\vec{c}}{v}$$

$$\vec{b}^* = \frac{\vec{c}\times\vec{a}}{v} \qquad (2.5)$$

$$\vec{c}^* = \frac{\vec{a}\times\vec{b}}{v}$$

where $v = \vec{a}\cdot(\vec{b}\times\vec{c}) = b\cdot(\vec{c}\times\vec{a}) = \vec{c}\cdot(\vec{a}\times\vec{b})$ and represents the volume of the unit cell.

Then

$$\vec{S} = h\vec{a}^* + k\vec{b}^* + \ell\vec{c}^* \qquad (2.6)$$

Since $\vec{S}$ was defined as the scattered vector each point in the reciprocal lattice is related to the direction of the diffracted beam relative to the incident beam.

Atomic scattering factor

Until now we assumed the scattering units to be electron in order that their linear dimensions could be neglected in comparison with the space lattice dimensions and also in comparison with the wavelength of the x-rays. Under these conditions the scattering by a single electron is independent of angle apart from any effects of polarization of the radiation. In atoms, however, the electrons occupy different positions and the phase differences between rays scattered from different points in this volume have to be taken into account. Thus the ratio of scattering in the direction $\vec{S}$ by an atom at the origin to that of an electron at the origin is given by:

$$f_j^o = \int \rho(\vec{r}) \exp(2\pi i \vec{S}\cdot\vec{r}) d\vec{r} \qquad (2.7)$$

and is called the atomic scattering factor f_j^o. It is evaluated theoretically for an atom at rest i.e. at absolute zero. The electron density function $\rho(\vec{r})$ is calculated theoretically assuming atoms to have a spherical symmetry. In this condition the atomic scattering factor is constant for a given angle of diffraction ($|S| = \frac{\sin\theta}{\lambda}$). The curve of scattering factor against $\frac{\sin\theta}{\lambda}$ is called the scattering factor curve or f curve and they are tabulated in the International Tables for X-ray Crystallography (24). Suppose now that the unit cell of a crystal contains N atoms, situated at the points x_j, y_j, z_j. The position of the nth atom in

the unit cell can thus be represented by the vector $\vec{r}_j$ where

$$\vec{r}_j = x_j\vec{a} + y_j\vec{b} + z_j\vec{c} \qquad (2.8)$$

For this atom the scattering contribution relative to an electron at the origin will be

$$\int \rho(\vec{r})\exp(2\pi i\vec{S}(\vec{r}+\vec{r}_j))d\vec{r} = f_j^o\exp(2\pi i\vec{S}\cdot\vec{r}_j). \qquad (2.9)$$

If all the atoms in the unit cell are considered the following expression is obtained:

$$F(\vec{S}) = \sum_{j=1}^{N} f_j^o\exp(2\pi i\vec{S}\cdot\vec{r}_j) \qquad (2.10)$$

This is the structure factor for the cell. A more exact expression can be obtained by replacing the assumption of zero thermal motion with a term accounting for the average displacement from the mean position due to thermal motions of the atoms. Thus the value of f_j is reduced in the following manner:

$$f_j = f_j^o \exp(-B_j \cdot \frac{\sin^2\theta}{\lambda^2}) \qquad (2.11)$$

where B_j is a positive definite quantity called the isotropic temperature factor and is related to the mean square amplitude of vibration $\overline{U_j^2}$

$$B_j = 8\pi^2\overline{U_j^2} \qquad (2.12)$$

This expression can be changed to account for anisotropic thermal vibration. When we refer to the reciprocal lattice axes the exponential can be expanded (due to equality - $B\frac{\sin^2\theta_{hk\ell}}{\lambda^2} = \frac{B}{4}\left(\frac{1}{d_{hk\ell}}\right)^2$)

$$\exp\left[-\frac{1}{4}(B_{11}h^2a^{*2}+B_{22}k^2b^{*2}+B_{33}\ell^2c^{*2}+2B_{12}hka^*b^*+2B_{13}h\ell a^*c^*+2B_{23}k\ell b^*c^*\right]$$

where the B_{ij} are the thermal parameters which are evaluated for each atom during the refinement of the crystal structure. If we substitute into the structure factor expression the value of r_j from equation (2.8) we have:

$$F_{hk\ell} = \sum_{j=1}^{N} f_j \exp 2\pi i (x_j\vec{a}\cdot\vec{S} + y_j\vec{b}\cdot\vec{S} + z_j\vec{c}\cdot\vec{S}) = \tag{2.13}$$

$$= \sum_{j=1}^{N} f_j \exp 2\pi i (hx_j + \ell y_j + \ell z_j)$$

(using the Laue's equations). This is the most common form for the structure factor expression. Its modulus is called the structure amplitude and is defined as the ratio of the amplitude of the radiation scattered in the order h,k,ℓ by the contents of one unit cell to that scattered by a single electron under the same conditions.

The complex form of structure factor expression can be given as:

$$F = A + iB \tag{2.14}$$

where A and B are defined:

$$A_{hk\ell} = \sum_j f_j \cos 2\pi (hx_y + ky_j + \ell z_j) \quad (2.15)$$

$$B_{hk\ell} = \sum_j f_j \sin 2\pi (hx_j + ky_j + \ell z_j). \quad (2.16)$$

Accordingly the magnitude and the phase α will be given:

$$|F_{hk\ell}| = \sqrt{A^2_{hk\ell} + B^2_{hk\ell}} \quad (2.17)$$

$$\alpha_{hk} = \tan^{-1} \left(\frac{B_{hk\ell}}{A_{hk\ell}}\right) \quad (2.18)$$

Thus far the structure factor has been considered as a resultant of adding the waves scattered in the direction of the hkℓ plane from the j atoms in the unit cell. This approach was based on a set of point atoms with variable scattering factors. A more fundamental interpretation of the structure factor is possible by considering the structure factor as the sum of the wavelets scattered from all infinitesimal elements of electron density in a unit cell with no assumptions about the distribution of this density. If ρ is the electron density the number of electrons in any volume element dv is

$$\rho(xyz)dv. \quad (2.19)$$

The wavelet scattered by this element is:

$$\rho(x,yz)\exp(2\pi i(hx+ky+\ell z))dv \quad (2.20)$$

The summation over all the elements in the unit cell gives the structure factor equation

$$F_{hk\ell} = \int_v \rho(xyz)\exp(2\pi i(hx+ky+\ell z))dv. \quad (2.21)$$

Since a crystal is periodic in three dimensions any three dimensional periodic function in a crystal can be represented by a three dimensional Fourier series. Thus electron density function can be written as:

$$\rho(xyz) = \sum_{h'} \sum_{k'} \sum_{\ell'} C_{h'k'\ell'} \exp 2\pi i(h'x+k'y+\ell'z) \qquad (2.22)$$

where each summation is between $-\infty$ and ∞.

Substitution of equation (2.22) in (2.21) gives:

$$F_{hk\ell} = \int_V \sum_{h'} \sum_{k'} \sum_{\ell'} C_{h'k'\ell'} \exp 2\pi i[(h+h')x+(k+k')y+(\ell+\ell')z]dv \qquad (2.23)$$

The exponential is periodic and the integral over one period is zero for all terms except that one for which $h'=-h$, $k'=-k$, $\ell'=-\ell$. In this case the periodicity disappears and:

$$F_{hk\ell} = \int_V C_{\overline{hk\ell}} dr = VC_{\overline{hk\ell}} \qquad (2.24)$$

$$C_{\overline{hk\ell}} = \frac{1}{V} F_{hk\ell} \qquad (2.25)$$

Substitution in eq. (2.22) of $\overline{hk\ell}$ for $h'k'\ell'$ and of $C_{\overline{hk\ell}}$ from equation (2.25) gives the required series:

$$\rho(xyz) = \frac{1}{V} \sum_{h} \sum_{k} \sum_{\ell} F_{hk\ell} \exp -2\pi i(hx+ky+\ell z)) \qquad (2.26)$$

Comparison of the expression for the electron density, equation (2.26) with that for structure factors equation (2.21) shows that the electron density is the Fourier transform of the structure factors while the structure factors are in turn the Fourier transform of the electron density.

An alternative expression for a three dimensional Fourier series can be obtained by noting that the structure factor can be written in the form:

$$F_{hk\ell} = |F_{hk\ell}| \exp^{2\pi i \alpha_{hk\ell}} \qquad (2.27)$$

where $2\pi\alpha_{hk\ell}$ is the phase angle.

Substituion in equation (2.26) gives

$$\rho(xyz) = \frac{1}{V} \sum_h \sum_k \sum_\ell |F_{hk\ell}| \exp^{-2\pi i (hx+ky+\ell z-\alpha_{hk\ell}))} \qquad (2.28)$$

It may be thought from the above expressions that the process of determining the crystal structures is completely obvious: from the observed values of intensities the values of the structure amplitude calculated and finally the electron density can be obtained. That this is not possible appears from the expression of the intensities which contain only the modulus of $F_{hk\ell}$:

$$I_{hk\ell} = c(L \cdot p) A(\theta) |F_{hk\ell}|^2 \qquad (2.29)$$

where c is a constant dependent on the intensity and wavelength of the incident radiation, and on the volume of the unit cell.

Since the crystals used in practice are actually mosaic there is a finite range of angle over which one can get diffraction maxima. L is the Lorentz factor and normalizes the speed with which reciprocal lattice points pass through the sphere of reflection (depends on position and direction in which they approach the sphere); p the polarization factor is a simple geometric factor and corrects for the partial

polarization of the x-ray beam. The term A accounts for the attenuation of both the incident and diffracted beams as they pass through the crystal mass and depends on the absorbing properties of the constituents in the crystal. Thus no direct information about the phase of a reflection is obtained by a measurement of its intensity. As we have seen, the use of expressions (2.26) and (2.28) for electron density imply the knowledge of absolute values. Thus in general, the process of solving a crystal structure cannot be carried out by direct means. A method to overcome this difficulty is shown in the next paragraph.

The Patterson function

Patterson showed (25) that a Fourier calculation can be carried out using phaseless quantities $|F_{hk\ell}|^2$ as the coefficients; these quantities are directly related to the observed intensities and so they can always be measured. Patterson defines a function P(u,v,w) such that

$$P(u,v;w) = \iiint \rho(xyz)\,\rho(x+u,y+v,z+w)\,dxdydz \qquad (2.30)$$

If we substitute in this expression the values for the electron densities given by equation (2.26) we arrive at the expression

$$P(u,v,w) = \frac{1}{V} \sum_h \sum_k \sum_{\ell=-\infty}^{+\infty} F_{hk\ell}\, F_{\overline{hk\ell}} \exp 2\pi i(hu+kv+\ell w) \qquad (2.31)$$

or

$$P(u,v,w) = \frac{1}{V} \sum_h \sum_k \sum_{\ell=-\infty}^{+\infty} |F_{hk\ell}|^2 \exp 2\pi i(hu+kv+\ell w). \qquad (2.32)$$

Patterson showed that this function has maxima corresponding to vector separations between atoms in the unit cell. Thus a peak at the point uvw in a Patterson map indicates that there exist in the crystal atoms at $x_1y_1z_1$ and $x_2y_2z_2$ such that

$$\begin{aligned} u &= x_1 - x_2 \\ v &= y_1 - y_2 \\ w &= z_1 - z_2. \end{aligned} \tag{2.33}$$

This is the importance of the Patterson series: it gives information about interatomic distances, but not about atomic positions. Since $p(u,v,w) = p(-u,-v,-w)$,

$$P(u,v,w) = \frac{1}{V} \sum_h \sum_k \sum_{\ell=-\infty}^{+\infty} |F_{hk\ell}|^2 \cos 2\pi(hu+kv+\ell w) \tag{2.34}$$

which is real for all values of u,v,w . $|F_{hk\ell}|^2$ has been shown to be proportional to the intensity $I_{hk\ell}$ at each reciprocal lattice point and $\langle|F_{hk\ell}|^2\rangle$ over all values of $\sin\theta/\lambda$ is equal with the summation over all the values of scattering factors f_j in the cell: i.e.

$$\overline{I_{hk\ell}} = \sum_{j=1}^{N} f_j^2 \tag{2.35}$$

which in turn are proportional with the number of electrons of the jth atom (see eq. (2.7)). Thus vectors between heavy atoms will give larger maxima than vectors between light atoms. That is, the height of a peak is proportional to the product of the atomic numbers of the atoms which are associated with the given vector.

The Patterson function contains the vector set $r_i - r_j$ and we want to find out the unique set r_i. This task will be easier to resolve when the structure contains a small number of heavy atoms. Light atoms may be resolved by their interaction with any heavy atoms in the structure but they present many more difficulties in the identification of superimposed peaks.

For a molecule containing N atoms per unit cell, the Patterson map will show N^2 peaks corresponding to the N possible vectors which can be drawn from each of the N atoms. Of these, N will be vectors of zero length from each atom to itself and will be represented (in a two dimensional map) as a large peak at the origin. The remaining N^2-N peaks will be distributed throughout the cell. Since the cell of the Patterson synthesis is the same size as that of the crystal the peaks are more closely packed and also many of them overlapped. Another feature of the Patterson peaks which results automatically by their construction is that their breadth is larger than that of the atoms contributing to the peaks. We should mention however, that the summation over h, k and ℓ in Patterson synthesis should extend from $-\infty$ to $+\infty$ and for this reason the maps produced with limited data may be subject to series termination errors and thus present further difficulties in resolution of small peaks.

The symmetry of the Patterson map is not the same as that of the real lattice. From the definition of the Patterson

function it follows immediately that all the Patterson maps are centrosymmetric. It can also be shown that to pass from real space group to the Patterson space group one must replace all translational symmetry elements (screws axes and glide planes) by the corresponding nontranslational ones (rotation axes and mirror planes).

Anomalous scattering

In the treatment of the structure factors, we have assumed that the scattering factors, f_j, are represented by real numbers. This is in general true because the values commonly used are calculated on the assumption that the frequency of the incident radiation differs widely from that of any natural absorption frequency of the atoms. (In this case the bound electrons behave like free electrons.) If the frequency of the incident beam does fall near a natural absorption frequency an anomalous phase change occurs during scattering by the innermost electrons whose frequencies are near the absorption edge. In this case, it can be shown from classical theory of scattering that the atomic scattering factor may be written:

$$f = f_o + \Delta f' + i\Delta f'' \qquad (2.36)$$

where f_o is the normal scattering, $\Delta f'$ is a real correction term (usually negative) and $\Delta f''$ is the imaginary component. Values of $\Delta f'$ and $\Delta f''$ for various elements and wavelengths have been tabulated in the International Tables for X-ray Crystallography (24).

An important consequence of anomalous scattering is that it causes a breakdown of Friedel's law which states that the diffraction pattern has a center of symmetry independent of whether the crystal does, i.e.

$$|F_{hk\ell}| = |F_{\bar{h}\bar{k}\bar{\ell}}|.$$

Let us consider the case of non-centrosymmetrical structure. We have

$$\begin{aligned} F(\vec{S}) &= \sum_j (f_j' + f_j'')\exp(2\pi i\, \vec{S}\cdot\vec{r}_j) \\ F(-\vec{S}) &= \sum_j (f_j' + if_j'')\exp(-2\pi i\vec{S}\cdot\vec{r}_j). \end{aligned} \tag{2.37}$$

From (2.37) it follows that

$$F(-\vec{S}) \neq F^*(\vec{S})$$

and

$$|F(\vec{S})|^2 \neq |F(-\vec{S})|^2$$

This important result gives another method for solving crystal structures. Let us write the scattering factor of an atom as:

$$f_j = f_j^R + i\Delta f_j \tag{2.38}$$

where the imaginary component is non zero only for an anomalous scatterer and is $\Delta f''$ of equation (2.36) and the real component for an anomalous scatterer f_j^R differs slightly from the non-anomalous value and is $f_o + \Delta f'$ of the same equation.

The structure factor of index S can now be written

$$F(\vec{S}) = \sum_{j=1}^{N} (f_j^R + i\Delta f_j)\exp(2\pi i\vec{S}\cdot\vec{r}_j) \tag{2.39}$$

The complex conjugate of $F(\vec{S})$ is given by:

$$F^*(\vec{S}) = \sum_{j=1}^{N} (f_j^R - i\Delta f_j)\exp(-2\pi i\vec{S}\cdot\vec{r}_j). \qquad (2.40)$$

From eqn. (2.39) and (2.40) we find:

$$|F(\vec{S})|^2 = F(\vec{S})\cdot F^*(\vec{S}) = \sum_j \sum_k (G_{jk} - iH_{jk})\exp(2\pi i\vec{S}(\vec{r}_j-\vec{r}_k) \qquad (2.41)$$

where the quantities G_{jk} and H_{jk} which are functions of $|S|$ are given by

$$G_{jk} = f_j^R f_k^R + \Delta f_j \Delta f_k$$
$$H_{jk} = f_j^R \Delta f_k - f_k^R \Delta f_j \; . \qquad (2.42)$$

Similarly we find that

$$|F(-\vec{S})|^2 = F(-\vec{S})\cdot F^*(-\vec{S}) = \sum_j \sum_k (G_{jk} + iH_{jk})\exp(2\pi i\vec{S}(\vec{r}_j-\vec{r}_k)) \qquad (2.43)$$

By combining (2.41) and (2.43) one obtains:

$$|F(\vec{S})|^2 + |F(-\vec{S})|^2 = 2 \sum_{j=1}^{N} \sum_{k=1}^{N} \{f_j^R f_k^R + \Delta f_j \Delta f_k\}\cos\, 2\pi\vec{S}\cdot(\vec{r}_j-\vec{r}_k) \qquad (2.44)$$

and

$$|F(\vec{S})|^2 - |F(-\vec{S})|^2 = 2 \sum_{j=1}^{N} \sum_{k=1}^{N} \{\Delta f_j f_k^R - \Delta f_k f_j^R\}\sin\, 2\pi\vec{S}\cdot(\vec{r}_j-\vec{r}_k) \qquad (2.45)$$

If in equation (2.44) we write $(\psi)_{\vec{S}} = \frac{1}{2}\{|F(\vec{S})|^2 + |F(-\vec{S})|^2\}$ then it is clear that $(\psi)_{\vec{S}}$ is the Sth Fourier coefficient of a function which has peaks at $\vec{r}_j-\vec{r}_k$. These peaks will have a Fourier transform which at the S-th point in reciprocal space has the values G_{jk}. This peak will be like a normal Patterson peak except that when one or both of the atoms is an anomalous scatterer the peak is very slightly modified

in weight and form. Thus the Fourier synthesis with $\frac{1}{V}(\psi)_{\vec{S}}$ as Fourier coefficients gives a function $P_e(\vec{r})$ which will be similar to a normal Patterson synthesis obtained with non anomalous scattering data except at points corresponding to the vectors involving anomalous scatterers. The function can be written:

$$P_e(\vec{r}) = \frac{1}{V} \sum_S \{|F(\vec{S})|^2 + |F(-\vec{S})|^2 \cos 2\pi\vec{S}\cdot\vec{r}. \qquad (2.46)$$

Similarly if we write $(\psi_o)_S = \frac{1}{2}\{|F(\vec{S})|^2 - |F(-\vec{S})|^2\}$ then $(\psi_o)_{\vec{S}} = -(\psi_o)_{-\vec{S}}$. Now it is clear that $(\psi_o)_{\vec{S}}$ is the Fourier coefficient of an odd function $P_o(r)$ which will have a peak corresponding to the transform of H_{gk} at $\vec{r}_j-\vec{r}_k$ and a peak corresponding to the transform $-H_{jk}$ at $-(\vec{r}_j-\vec{r}_k)$. The function is given by

$$P_o(\vec{r}) = \frac{1}{V} \sum_S \{|F(\vec{S})|^2 - |F(-\vec{S})|^2\}\sin 2\pi\vec{S}\cdot\vec{r}. \qquad (2.47)$$

Thus the peak is positive if $\vec{r}_j-\vec{r}_j$ is a vector from an anomalous atom k to a normal atom u, negative if the peak corresponds to a vector in the opposite direction and zero if the vector is between normal atoms, since these three possibilities correspond to $\Delta f_k > 0$ $\Delta f_j = 0$; $\Delta f_k = 0$ $\Delta f_j > 0$ and $\Delta f_k = \Delta f_j = 0$ respectively. Thus while the ordinary Patterson function contains N^2 peaks when there are N atoms per unit cell the odd Patterson function contains $n(N-n)$ positive peaks related to the same number of negative peaks by a center of symmetry, where n is the number of

anomalous atoms per unit cell.

It is worthwhile mentioning that accurate measurements of the differences between intensities $I_{hk\ell} - I_{\overline{hk\ell}}$, which would be equal in the absence of anomalous scattering, are therefore required.

Direct methods

Since 1960 many structures have been solved using direct methods of phase determination from the structure factors with the only postulate that the atoms are randomly distributed. A large number of formula for direct phase determination have been proposed. Most of them are based on the same fundamental principles but differ in the manner of handling the data and extracting the phases. We will confine our discussion to the method most often used and which appears to have general applicability - the symbolic addition procedure. We will also discuss only the centrosymmetric case in which the phasing consists simply of assigning a plus or minus sign to each observed structure amplitude or at least to the large terms in the electron density expression. The method is based on the fact that the electron density in a crystal is everywhere real, positive and continuous (the positivity criterion). On this basis, Karle and Hauptman (26) derived a complete set of inequalities which are valid for all the space groups. The first three are:

$$F_{ooo} \geq 0 \tag{2.47}$$

$$|F_{hk\ell}| \leq F_{ooo} \tag{2.48}$$

$$\left|F_{h_1\ h_2, k_1+k_2, \ell_1+\ell_2} - \frac{F_{h_1k_1\ell_1} F_{n_2k_2\ell_2}}{F_{ooo}}\right| \leq \frac{\left|\begin{matrix} F_{ooo} & F_{\bar{h}_1\bar{k}_1\bar{\ell}_1} \\ F_{h_1k_1\ell_1} & F_{ooo} \end{matrix}\right|^{\frac{1}{2}} \left|\begin{matrix} F_{ooo} & F_{\bar{h}_2\bar{k}_2\bar{\ell}_2} \\ F_{h_2k_2\ell_2} & F_{ooo} \end{matrix}\right|^{\frac{1}{2}}}{F_{ooo}} \tag{2.49}$$

Equations (2.47) and (2.48) are trivial statements. For the case of crystals having a small number of atoms, the third relation (2.49) can provide a basis for phase determination in both centrosymmetric and noncentrosymmetric crystals. We can rewrite (2.49) in the form:

$$|F_{\vec{h}} - \delta| \leq r \tag{2.50}$$

where

$$\delta = \delta\ (h,k) = F_{\vec{h}-\vec{k}}\ F_{\vec{k}}/F_{ooo} \tag{2.51}$$

$$r = \frac{\left|\begin{matrix} F_{ooo} & F^{*}_{\vec{h}-\vec{k}} \\ F_{\vec{h}-\vec{k}} & F_{ooo} \end{matrix}\right|^{\frac{1}{2}} \left|\begin{matrix} \frac{1}{2} F_{ooo} & F^{*}_{\vec{k}} \\ F_{\vec{k}} & F_{ooo} \end{matrix}\right|^{\frac{1}{2}}}{F_{ooo}} \tag{2.52}$$

and $\vec{h} = \vec{h}_1 + \vec{h}_2$, $\vec{k} = \vec{h}_2$. Here the symbol $\vec{h}$ denotes the vector $h\vec{a}^* + k\vec{b}^* + \ell\vec{c}^*$.

Karle and Karle (27) pointed out that equation (2.50) implies that the complex structure factor $F_{\vec{h}}$ is bounded by a circle in the complex plane whose center is δ and whose radius is r. If the magnitude of $F_{\vec{h}}$ is known, it will be restricted to the arc values within the circle of radius r. The larger

the values of $|F_{\vec{k}}|$ and $|F_{\vec{h}-\vec{k}}|$, the smaller will be r, and the closer will $F_{\vec{h}}$ be to the complex number δ. Since the vector $\vec{k}$ can be varied arbitrarily, many different relations of the type (2.50) would exist. Forlarge $|F_{\vec{k}}|$, $|F_{\vec{h}-\vec{k}}|$, the quantities $\delta(\vec{h},\vec{k})$ would cluster in a particular region of the complex plane, and $F_{\vec{h}}$ would be located within this cluster. ($F_{\vec{h}}$ will lie within the intersection of several circles, each with a new δ and a new r). Thus $F_{\vec{h}}$ will be proportional to an average over the various $\delta(\vec{h},\vec{k})$ involving the large $|F_{\vec{k}}|, |F_{\vec{h}-\vec{k}}|$ values as $\vec{k}$ is varied:

$$F_{\vec{h}} \approx \langle F_{\vec{k}} F_{\vec{h}-\vec{k}} \rangle_{\vec{k}} \quad . \tag{2.53}$$

Defining the phase of the structure factor like we did before (Eq. 2.27):

$$F_{\vec{h}} = |F_{\vec{h}}| \exp(i\phi_{\vec{h}})$$

then for $F_{\vec{h}}$, $F_{\vec{k}}$ and $F_{\vec{h}-\vec{k}}$ of large magnitude we have approximately:

$$\phi_{\vec{h}} \approx \langle \phi_{\vec{k}} + \phi_{\vec{h}-\vec{k}} \rangle_{\vec{k}} \tag{2.54}$$

since

$$\delta(\vec{h},\vec{k}) = |\delta(\vec{h},\vec{k})| \exp[i(\phi_{\vec{k}} + \phi_{\vec{h}-\vec{k}})] . \tag{2.55}$$

As the complexity of the structure increases, the fraction of the total number of electrons contributing to a given reflection will on average, decrease. Thus r increases and inequality (2.50) gives less information and finally imposes no restriction on the phase of $F_{\vec{h}}$. It can be shown using arguments based on probability theory that equation (2.54) still holds and it is possible to obtain additional useful phase determining relations.

An outline of the approach developed by Karle, Hauptman and others is given in the following paragraphs.

Normalized structure factors

Normalized structure factors (E'S) have been proved useful in direct methods (27). They may be defined:

$$|E_{\vec{h}}|^2 = \frac{c|F_{\vec{h}}|^2}{\varepsilon \sum_{j=1}^{N} f_j^2} \qquad (2.56)$$

where

$$|E_{\vec{h}}| = E_h \exp(i\phi_h) \qquad (2.57)$$

$F_{\vec{h}}$ is a structure factor corrected for thermal motion, f_j is the atomic scattering factor for the jth atom in a unit cell containing N atoms, c is a scale factor (28) such that the average value of $\langle|E|\rangle^2 = 1.00$ and ε is a number which corrects for space group extinctions.

Physically the $|E|$-values are the structure factors for the fully sharpened atoms. A Fourier synthesis constructed (with the correct phases) and the infinite set of $|E|$ values as Fourier coefficients will show Dirac δ function peaks at the position of the atom centres provided that all the atoms have identical scattering factors. For structures in which temperature factors are strongly anisotropic, the normalization procedure of eq. (2.56) is not adequate and anisotropic corrections are needed. The approach outlined below is due to Maslen (29) and was used in the attempt at a structure determination of $Ca_2V_2O_7$ described in Chapter 3.

$F_{hk\ell}$ in eqn. (2.56) is the structure factor on an

absolute scale defined by

$$|F_{hk\ell}| = |F_{rel\ hk\ell}| K(S) \exp(M+J) \qquad (2.58)$$

where $S = \sin\theta/\lambda$, $|F_{rel\ hk\ell}|$ is derived from the experimentally measured intensity $I_{hk\ell}$ using eq, (2.29) and K(S) is the K curve , i.e. the Wilson plot with isotropic correction (30) drawn for 19 equal volume overlapping regions of reciprocal space. M is an overall isotropic temperature factor, and J gives anisotropic temperature corrections thus:

$$J = \alpha_{11}h^2 + \alpha_{22}k^2 + \alpha_{33}\ell^2 + \alpha_{12}hk + \alpha_{13}h\ell + \alpha_{23}k.$$

The values of the α's are obtained by a least squares fit to a plot of

$$n\left[\frac{\sum_{h,k,\ell}\sum_{j=1}^{N} m\varepsilon f_j^2}{\sum_{h,k,\ell} m|F_{rel\ hk\ell}|^2 K^2(S)\exp(2M)}\right]$$

against h^2 for α_{11}, k^2 for α_{22}, ℓ^2 for α_{33}, hk for α_{12}, $h\ell$ for α_{14}, $k\ell$ for α_{23}. Here $m = m(hk\ell)$ is the multiplicity factor. The summations over h,k,ℓ are within one of the 19 volumes of the reciprocal space.The values of the α's are iterated five times to obtain reliable estimates.

Probability considerations

The significance of equation (2.53) for phase determination was pointed out by Karle and Hauptman (26) in 1950.

The use of (2.53) for sign determination in centrosymmetric crystals was established by Sayre (31) who has shown

that the sign of $F_{\vec{h}}$ would almost certainly be the same as of the product $F_{\vec{k}} \cdot F_{\vec{h}-\vec{k}}$ if large structure factor magnitudes were involved:

$$S(F_{\vec{h}}) \sim S(F_{\vec{k}}) \cdot S(F_{\vec{h}-\vec{k}}) \tag{2.59}$$

where S means "sign of" and $\sim$ means "is probably equal to". The final formula used in phase determination was derived by Hauptman and Karle (32) using normalized structure factors

$$SE_{\vec{h}} \sim S \sum_{k} E_{\vec{k}} E_{\vec{h}-\vec{k}} \tag{2.60}$$

where k implies only the summation over those vectors associated with large $|E|$ values. This formula was termed Σ_2 and it is the probability equation of the inequality (2.50) (ibidem).

The associated probability function $P_+(E_h)$ which determines the probability that the sign of E_h will be positive was given by different authors in various forms but the most commonly used is the hyperbolic tangent form obtained by Woolfson (33)

$$P_+(E_{\vec{h}}) = \frac{1}{2} + \frac{1}{2} \tanh \sigma_3 \sigma_2^{-3/2} |E_{\vec{h}}| \sum_{k} E_{\vec{k}} E_{\vec{h}-\vec{k}} \tag{2.61}$$

where P_+ is the probability that the equation (2.56) will hold and

$$\sigma_n = \sum_{j=1}^{N} z_j^n \,. \tag{2.62}$$

z_j is the atomic number of the jth atom.

Since the argument of the hyperbolic tangent in eq. (2.61) can be either positive or negative, depending on the

sign of the summation of the E products, the values of $P_+(E_{\vec{h}})$ can range between 0 (Σ = large negative) and 1 (Σ = large positive). Values of P_+ less than $\frac{1}{2}$ are thus indications that the sign of $E_{\vec{h}}$ is negative with a probability P_- given by

$$P_- = 1 - P_+. \tag{2.63}$$

Given a properly chosen set of specified signs and unknown symbols, we expand and refine the set using equations (2.60) and (2.61). The phase set is then used to compute an E map in which peaks should show the atomic positions.

Invariants and semi-invariants

To use equation (2.60) we must first have a starting set of phases $\phi_{\vec{k}}$, $\phi_{\vec{h}-\vec{k}}$ in order to determine $\phi_{\vec{h}}$. In this section we discuss the restrictions on the hkℓ indices and on the values of the starting phases.

To determine which phases may be specified, we make use of the theory of structure invariants and structure semi-invariants (32). The general expression for the structure factor for a structure with N atoms in the unit cell was given:

$$F_{hk\ell} = \sum_{j=1}^{N} f_j \exp[2\pi i(hx_j+ky_j+\ell z_j)]. \tag{2.13}$$

If the origin is shifted to a different point having coordinates $x_o\ y_o\ z_o$ with respect to the first origin then x_j, y_j, z_j, in (2.13) are replaced by x_j-x_o, y_j-y_o, z_j-z_o. It is readily verified that this is then replaced by:

$$F'_{hk\ell} = F_{hk\ell} \exp[-2\pi i(hx_o+ky_o+\ell z_o)].$$

Thus the magnitude of $F_{hk\ell}$ remains unchanged while the phase $\phi_{hk\ell}$ of $F_{hk\ell}$ is replaced by

$$\phi'_{\vec{h}} = \phi_{\vec{h}} - 2\pi(hx_o + ky_o + \ell z_o). \qquad (2.64)$$

From these equations we see that the crystal structure alone does not determine the values of all the phases since eq. (2.13) implies that an appropriate origin has been selected.

In principle, we could define any point to be the origin, but in practice the structure will be most easily solved if we make full use of symmetry and select an origin from among the restricted number of points which preserves the full symmetry of the space group. These points are called the permissible origins. The concept of equivalent origins leads to the notion of equivalence classes. Origins within the same equivalence class are related in the same manner to the symmetry elements of the space group. Hauptman and Karle (32) showed that there always exist certain linear combinations of the phases whose values (reduced modulo 2π) depend upon the structure alone and are independent of the choice of permissible origin. These linear combinations of phases are called structure invariants. Further for a given class of equivalent origins (in other words for a fixed functional form of the structure factor) there always exist certain linear combinations of the phases called structure semi-invariants whose values, reduced modulo 2π, depend upon the structure alone and are independent of the choice of

origin within the equivalence class.

Evidently every structure invariant is also a structure semi-invariant. In fact those structure semi-invariants whose values are independent of the chosen functional form for the structure factor coincide with the structure invariants.

To illustrate these concepts we take the example of the triclinic space group $P\bar{1}$. For this space group as for all primitive centrosymmetric space groups the permissible origins are defined to be eight points of the type ε_1, ε_2, ε_3 where $\varepsilon_i = 0$ or $\frac{1}{2}$, $i = 1,2,3$ which coincide with the centers of symmetry. Written in full they are:

$$(0,0,0), (\tfrac{1}{2},0,0), (0,\tfrac{1}{2},0), (0,0,\tfrac{1}{2}), (\tfrac{1}{2},\tfrac{1}{2},0), (\tfrac{1}{2},0,\tfrac{1}{2}), (0,\tfrac{1}{2},\tfrac{1}{2}), (\tfrac{1}{2},\tfrac{1}{2},\tfrac{1}{2}).$$

Since all eight permissible origins are equivalent, the distinction between invariants and semi-invariants disappears in this space group and only semi-invariants will be discussed.

Using equation (2.64) and the allowed permissible origins we see that all reflections with h even, k even, ℓ even are semi-invariant. For this space group the vector semi-invariantly associated with $\vec{h}(\equiv hk\ell)$ is (h,k,ℓ) and the semi-invariant modulus ω_s is $(2,2,2)$. From equation (2.59) it is seen that when the phase of a reflection has been specified the phase of all reflections equivalent to it are also fixed for a known structure. Thus all the reflections within the experimental sphere may be used in the phase determination process, not just the independent ones.

Karle and Hauptman (32) specified restrictions on the indices hkℓ of the reflections to be select to define the origin. We specify the maximum number of phases (three for $p\bar{1}$ which are linearly semi-independent, i.e. which do not combine to give a semi-invariant. We then use the set of Σ_2 relationships given by equation (2.60) to generate the phases of more reflections with large $|E|$ values. This set of phases together with some additional symbols are assigned in a step-by-step fashion to generate the phases of all reflections with $|E|$ values over a given threshold ($|E| \geq 1.50$). The application of the method to the structure in question is described in Chapter 3.

CHAPTER III

STRUCTURE OF CuV_2O_6

EXPERIMENTS

The compound was prepared in accordance with the phase diagram of CuO and V_2O_5 (34). The phase diagram shows five invariants plateaux (see Fig. 3-1). They correspond to three eutectics and two peritectics.

Our compound corresponds to 1:1 molar ratio and has a melting point of $\sim$ 640°C. Crystals were grown in oxygen atmosphere to avoid "bronze" formation in V_2O_5 rich regions and also to avoid CuO decomposition in the regions where the last one is rich. (Vanadium oxygen bronzes are well defined compounds of the form $M_xV_2O_5$ or $M_xV_3O_8$ in which vanadium exists in the IV and V oxidation states (e.g. $Cu_xV_2O_5$ $0.24 \leq x \leq 0.64$)

The material used to prepare crystals of CuV_2O_6 was a mixture of 1:1 molar ratio of V_2O_5 and CuO oxide of high purity (CuO - Merck 99.97% and V_2O_5 Fisher 99.99%). To get uniform size distribution each powder separately was ground in an agate mortar for some time ($\frac{1}{2}$ hour). After weighting the mixture was homogenized in a closed bottle for 12 hours using the rotational movement of a lathe. From time to time the lathe was stopped and the powder stuck on the walls removed.

Figure (3-1)

Phase diagram for the system $CuO-V_2O_5$

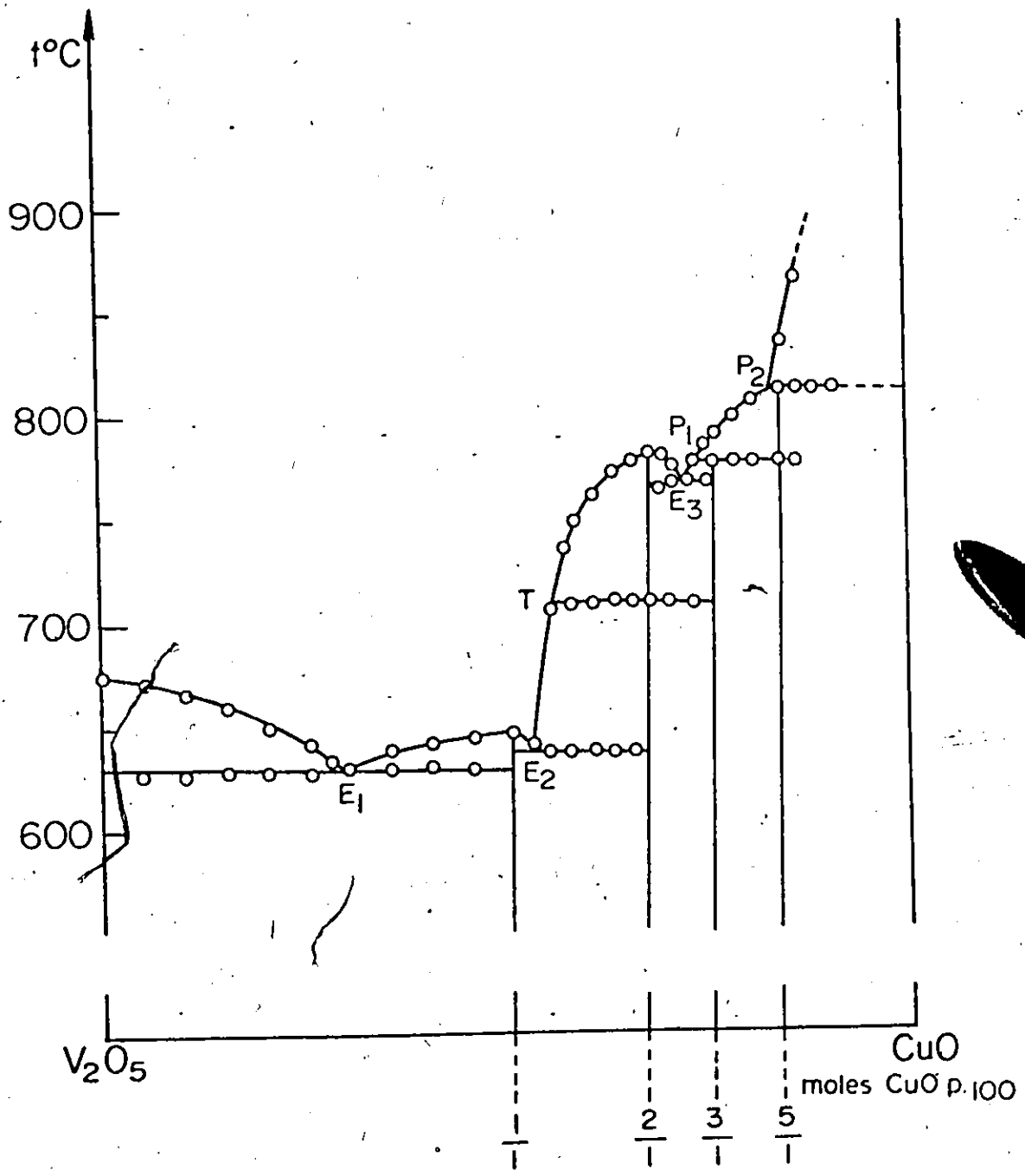
t°C
900
800
700
600
P2
P1
E3
T
E1
E2
V2O5
CuO
moles CuO p. 100
1/1
2/1
3/1
5/1

In this manner a homogeneous sample was obtained. This improvised method was used because we don't find an adequate mill with balls for grinding and homogenizing the material. All these precautions were necessary especially due to configuration of the phase diagram (V_2O_5 melts at 690°C and CuO at 1326°C).

The mixture was then heated for 12 hours at 800°C in an oxygen atmosphere, in a platinum crucible and cooled at a rate of 3°C/hr to 590°C. The crucible was taken from the furnace and air quenched. A microscopic examination of the sample showed that a substantial number of single crystals were obtained. The crystals were red-black and irregularly shaped.

One crystal was chosen for diffraction work, some portion of the others used to run a Debye-Scherrer pattern.

Precession photographs showed that the crystal crystallizes in triclinic system with space group $C\bar{1}$. ($C\bar{1}$ is an unconventional setting of $P\bar{1}$ space group chosen in this particular case in order to get lattice parameters parallel and commensurate with the other metavanadate structures in this series, eg. MgV_2O_6, ZnV_2O_6, CdV_2O_6.) The following systematic absence was observed $hk\ell$: $h+k = 2n+1$ (odd) where n is an integer. The unit cell parameters as determined from a least squares fit to 12 2θ values are:

$a = 1.968(6)\text{Å}$ $b = 3.543(3)\ \text{Å}$ $c = 6.478(7)\text{Å}$

$\alpha = 92.25(8)°$ $\beta = 110.34(7)°$ $\gamma = 91.88(6)°$.

2θ values were obtained from a powder pattern using Debye-Scherrer camera (CuKα radiation). These data were indexed with a program (CHIANG) of X-ray 67 (35). The program gives d spacing functions of 2θ for a chosen cell. The index of the powder pattern is shown in the Table 3-1. The table also includes the x-ray intensities collected from single crystal data brought to a proper scale. The disagreement sometimes observed between intensities on powder pattern film and single crystal are due to the fact that the first ones were not corrected for Lorentz, polarization factors. Taking into account the precision of the instrument used for reading the powder pattern, the agreement between d observed and d calculated are very good. Some doublets can not be resolved on powder film and they appear like a unique line. A more suitable radiation should be used (chromium $\lambda = 2.29092$ Å) but the fluorescence of the sample prevents us from obtaining an accurate picture. However, the powder pattern shows clearly that the right compound was obtained.

The crystal chosen for x-ray diffraction work has dimensions $0.25 \times 0.1 \times 0.1$ mm^3. The crystal was mounted on a thin glass fibre on a Supper goniometer head for data collection on the Syntex automatic diffractometer.

Twelve reflections were centered automatically on the Syntex automatic diffractometer and precise angular coordinates found by least squares refinement. A total of 1163 reflections were measured of which 1060 were observed.

Table 3-1

CuV_2O_6 - powder pattern index (CuKα 28 KV - 14 mA 35 hours)

a = 9.168Å b = 3.543 Å c = 6.478 Å
α = 92.25 β = 110.34 γ = 91.88

hkℓ	d_{obs}	d_{calc}	I/I_o*
200	4.28	4.29	12
$\bar{2}01$		4.28	20
$\bar{1}10$	3.33	3.33	67
110	3.23	3.21	47
$\bar{1}\bar{1}1$	3.08	3.08	32
201	3.030	3.039	62
002		3.032	17
$1\bar{1}1$	2.818	2.819	65
111	2.649	2.650	60
$\bar{1}\bar{1}2$	2.425	2.435	35
$\bar{1}12$	2.332	2.342	25
$\bar{3}1\bar{1}$		2.329	67
$\bar{4}01$	2.284	2.290	48
$\bar{3}10$		2.280	35
$\bar{3}\bar{1}1$	2.256	2.271	60
$\bar{3}\bar{1}0$	2.183	2.172	34
202	2.143	2.148	29
400		2.146	42
$\bar{3}\bar{1}2$	2.086	2.085	27
$\bar{3}12$		2.082	46

(cont'd next page)

Table 3-1 (continued)

hkℓ	d_{obs}	d_{calc}	I/I_o*
003	2.022	2.021	63
$3\bar{1}1$	1.989	1.982	46
311	1.873	1.875	42
$\bar{1}\bar{1}3$	1.861	1.869	56
$\bar{4}03$	1.825	1.824	71
$\bar{1}13$	1.797	1.797	57
020	1.771	1.768	100
$3\bar{1}3$		1.766	10

*From single crystal measurements

(Reflections whose intensity corrected for background exceeded three times the calculated standard deviation (3σ), were considered observed; reflections with intensities smaller than 3σ were left out of the refinement.) The information was transferred from magnetic tape to cards and these cards were used as input for programs called DATCO3 and DATRN of X-ray 71 (35). These programs calculate the Lorentz and polarization corrections and F values from intensities and sort the data according to hkℓ indices. In addition they present a plot of standard reflection versus time. In addition using an effective diameter of 2R = 0.15 mm the linear absorption coefficient was calculated:

where $$\mu_\lambda = \rho_{CuV_2O_6} \sum_i g_i \left(\frac{\mu}{\rho}\right)_i$$

$\rho_{Cu_2V_2O_6}$ (calculated) = 4.35

g_i = mass fraction contributed by the element i

$\left(\frac{\mu}{\rho}\right)_i$ = mass absorption coefficient of the element i.

It is found that $\mu_\lambda = 102.48\ cm^{-1}$

and $\mu_\lambda R = 1.5.$

For $\mu_\lambda R = 1.5$ the values of A* taken from International Tables for X-ray Crystallography (36) are used to calculate the corrected values of F_{obs} in the program DATRN.

D. Lavaud and J. Galy (7) have reported on the structure of CuV_2O_6 and their results are the following:

Space group : C2 a = 9.18±0.01Å, b = 3.58±0.03Å, c = 6.48±0.01Å

β = 110.4°, Z = 2.

The assignment of C2 space group by the French authors appears erroneous because only 96 reflexions were recorded and only in planes perpendicular to the two fold axis (h0ℓ,h1ℓ,h2ℓ). For this reason the existence of this axis can not be really proven and also small deviations from perpendicularity ($\alpha \neq \gamma \neq 90°$) will not be observed. In fact in our triclinic space group found $C\bar{1}$, the angles are slightly different from 90° α = 92.25(3)°, γ = 91.88(6)°. It is worth mentioning that β angle in previous determination is nearly the same. The atomic parameters found by these authors are written in Table 3-2.

Table 3-2

Atomic Parameters in CuV_2O_6

(Lavaud and Galy (7))

Atom	x	y	z
Cu	0	0	0
V_1	0.1923	0.033	0.6523
O_1	0.030	-0.002	0.722
O_2	0.336	-0.003	0.883
O_3	0.308	-0.019	0.449

The atomic coordinates from Table 3-2 were used as the initial parameters in this refinement. Several cycles of least squares refinement were performed and the scale constant

positional parameters and anisotropic temperature factors were varied.

At this stage a weighting function $w = (1.0+0.5\,F_o +0.001\,F_o^{-2})^{-1}$ was chosen so that $w(|F_o|-|F_c|)^2$, the square of the difference between the observed and calculated structure factors, would be independent of the local average of $|F_o|$. A weighting scheme was used in order to give the same weight to the whole body of data, in this manner preventing the strong reflections at low angles (less inaccurate) to dominate the refinement. There was a small improvement in R_w. The anisotropic temperature factor changed considerably but the atomic distances shifted imperceptibly (i.e. fifth decimal place). Even after this correction was made, it was obvious that 2 reflections whose F_{obs} and F_{calc} values compared very unfavourably, were unreliable; hence these two reflections were labeled as unreliable and given zero weight in the least square refinement. The final R value was 0.047. The final parameters are given in Table 3-3. The observed and calculated structure factors are listed in Table 3-6.

DESCRIPTION AND DISCUSSION OF THE STRUCTURE

The structure can be described conveniently in terms of the octahedra of oxygen atoms about both the copper and vanadium atoms. Refer to Fig. 3-2 (ac projection) where the Cu atoms are situated at the four corners of the unit cell and half way up the a axis; approximately perpendicular to the ac plane and passing through each of these

Figure (3-2)

Structure of CuV_2O_6 projected normal to the ac plane. The small open circles are Cu atoms and the filled circles are vanadium atoms. The larger circles are oxygen atoms. The filled bonds indicate the V-O bonds of the VO_6 groups with V at $y = \frac{1}{2}$. The pseudo-tetrahedral group is outlined.

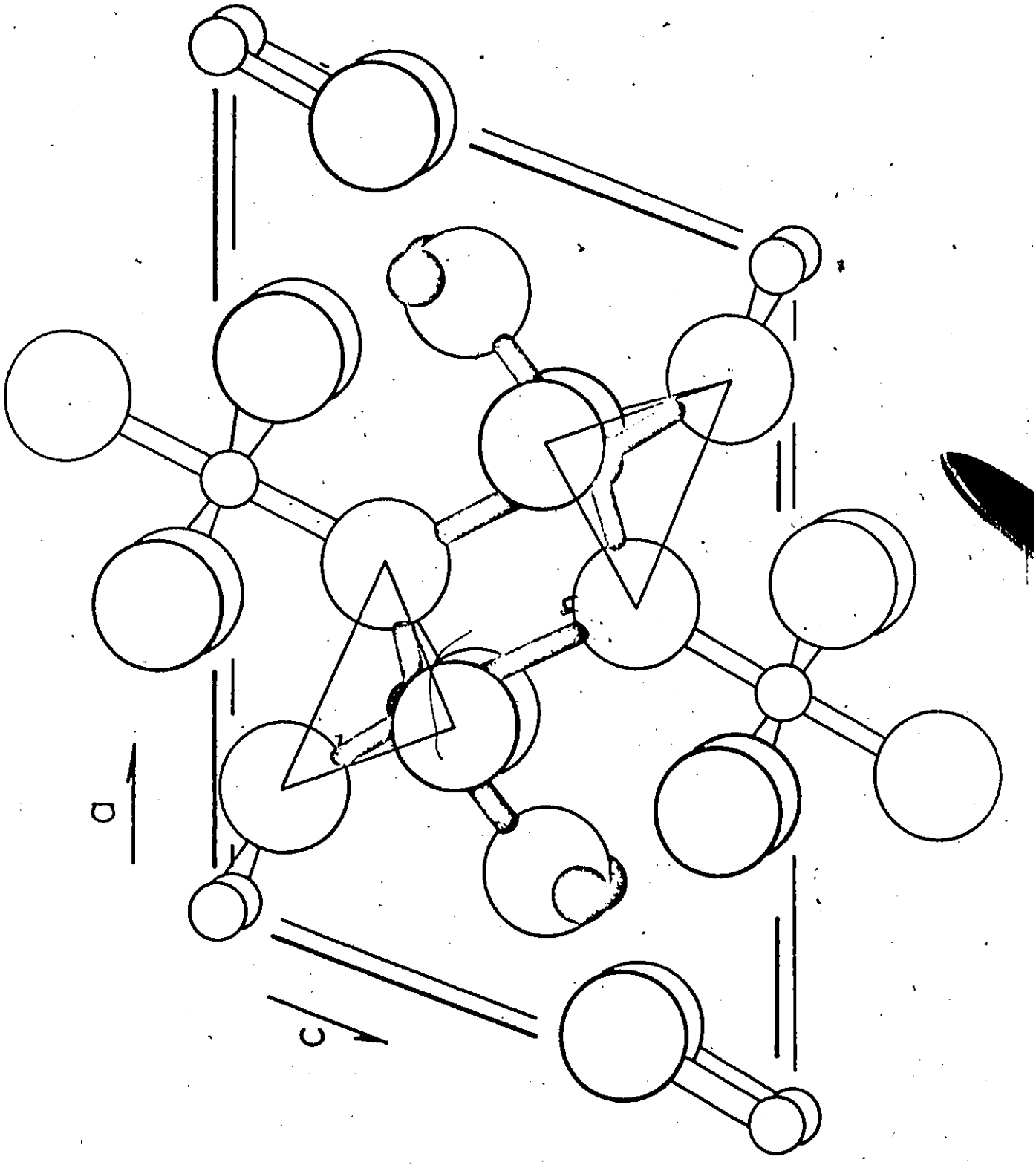
a
c

Table 3-3

Atomic Position and Thermal Parameters for CuV_2O_6

Atom	x	y	z	$u_{11}^{\dagger}(\text{Å})^2$	$u_{22}(\text{Å})^2$	$u_{33}(\text{Å})^2$	$u_{12}(\text{Å})^2$	$u_{13}(\text{Å})^2$	$u_{23}(\text{Å})^2$
Cu	0	0	0	0.0097(2)	0.0103(2)	0.0067(2)	0	0.0060(2)	0
V	0.19279(4)	0.01267(4)	0.65463(6)	0.0064(2)	0.0042(2)	0.0051(2)	0.0015(1)	0.0046(1)	0.0005(
O(1)	0.304(2)	0.0027(5)	0.7239(3)	0.0095(7)	0.0095(6)	0.0097(7)	-0.0000(5)	0.0079(5)	-0.006(5
O(2)	0.3426(2)	0.0482(6)	0.8896(3)	0.0103(7)	0.0114(7)	0.0079(7)	0.0007(5)	0.0038(5)	0.0007(
O(3)	0.3067(2)	-0.0028(5)	0.4316(3)	0.0094(7)	0.0046(5)	0.0091(7)	0.0021(4)	0.0067(5)	0.0011(

*Estimated standard derivations in parentheses.

†Calculated for $\beta_{ij} = 2\pi^2 b_i b_j U_{ij}$ where $T = \exp-(\beta_{11}h^2+2+\beta_{22}k^2 +\beta_{33}\ell^2+2\beta_{12}hk + 2\beta_{13}h\ell+ + 2\beta_{23}k\ell)$ is the thermal factor appearing in the structure factor expression and b_i's are the reciprocal lattice vectors.

points there are chains of CuO_6 octahedra propagating in the y direction. For example consider the Cu atom half way along the a axis; it is bonded to two O(2) atoms above the plane of $y \approx 1$ and to two O(2) atoms below the plane of $y \approx 0$. This octahedron shares an O(2)-O(2') edge with an octahedron above the plane and it also shares another one with an octahedran below the plane. Via these two shared edges, this octahedron forms a link in the chain of CuO_6 octahedra which propagate in the y direction. Interconnecting these chains are chains of VO_6 octahedra. Each octahedron shares three edges with other VO_6 groups. One shared edge is O(1)a-O(1)b which connects two VO_6 groups on one side of the chain. On the other side chains interleaf such that one octahedron shares two edges O(3)a-O(3)d and O(3)a-O(3)d' with two adjacent octahedra in a neighbouring chain. (These two octahedra are separated by a b axis length).

The latter two edges are the links in the VO_6 chains which propagate in the y direction whereas the former edge joins VO_6 groups related by the center of symmetry.

Although the Cu ion lies in an ordinary octahedral site albeit distorted in the closed packed array of oxygen atoms the V ion lies in a distorted tetrahedrally site formed with O(1), O(2), O(3) and O(3)d'. These four atoms lie between 1.655 and 1.871 Å of the vanadium ion. The O(3)-V-O(3)d' bond angle is enlarged to 144.9° in order to accomodate a fourth oxygen atom in the same layer and the sixth V-O bond

involves an interaction with an oxygen atom from another layer. These later bond lengths are 2.056(2)Å for V-O(3)a and 2.588 Å for V-O(1)b.

The elongated Cu-O(2)c',d' bonds 2.438 Å probably due to Jahn-Teller distortion destroy the mirror plane of the C2/m of isotypic MgV_2O_6 structure, while the Cu-O(1)a and Cu-O(1)b bonds contract to 1.904 Å in order to maintain the bond strength around the Cu^{2+} ion. If these latter bonds were to elongate the C2/m space group could be maintained but with serious underbonding of these oxygen atoms since they are bonded strongly to only one vanadium and weakly to a second.

The bond geometry is presented in Table 3-4.

The structure was tested for correctness using the bond strength-bond length relationship for oxides derived by Brown and Shannon (37). These relations were derived requiring that the sums of the bond strength around the cations be equal to their valence. They have analyzed environments of cations in 417 different structures and have derived R-S curves for M-O bonds for the majority of atoms in the first half of the periodic table in a simple two-parameter form.

The relationship is of the form: $S = S_o(R/R_o)^{-N}$ where S = bond strength, R = bond length and R_o and N are fitted constants (found by least square refinements). S_o, (the bond strength associated with a bond length R_o) is assigned arbitrarily.

Table 3-4

Bonding Geometry in CuV_2O_6

(Standard errors in parentheses)

bond		distance Å	angle	degree
Cu-O(1)a,b	2x	1.904(2)	O(1)a-Cu-O(2)c	90.9(1)
-O(2)c,d	2x	2.049(2)	-O(2)c'	87.1(1)
-O(2)c'd'	2x	2.438(2)	O(2)c -O(2)c'	104.0(1)
V-O(1)b		2.588(2)	O(1)b-V-O(3)a	76.3(1)
-O(3)a		2.056(2)	-O(1)a	77.0(1)
-O(1)a		1.697(2)	-O(2)a	175.6(1)
-O(2)a		1.655(2)	-O(3)d	80.9(1)
-O(3)d		1.871(2)	-O(3)d'	76.0(1)
-O(3)d'		1.845(2)	O(3)a-V-O(1)a	153.2(1)
			-O(2)a	100.6(1)
			-O(3)d	73.8(1)
			-O(3)d'	75.4(1)
			O(1)a-V-O(2)a	106.2(1)
			-O(3)d	99.8(1)
			-O(3)d'	100.2(1)
			O(2)a-V-O(3)d	101.5(1)
			-O(3)d'	100.2(1)
			O(3)d-V-O(3)d'	144.9(1)

It is important that this functional relationship relates bond strength to bond length regardless of structure type, with the constraint that the sum of the bond strength equals the valence as proposed by Pauling from 1929. It is also important that all ions with an isoelectronic core can be fitted by a single pair of parameters, R_o and N, that are independent of the ionic character of the bond and the coordination number of the cation.

An examination of the results for V^{5+} shows that the model works well, the average deviation from 5.00 being only 4.2%. We apply this relationship using the values given by Brown and Shannon for V^{5+} and Cu^{2+}. The bond strengths are determined from

$$S_{Cu^{2+}} = \frac{1}{3}\left(\frac{2.084}{R}\right)^{5.3} \quad , \quad S_{V^{5+}} = \frac{3}{4}\left(\frac{1.714}{R}\right)^{5.1} .$$

The results are shown in Table 3-5. The table shows that the bond strength sums around the cations lie within 5% of the valence. This can be considered as a test for correctness for a well refined structure. The discrepancies in bond strength sums should not surpass 5% of the valence. Table 3-5 also lists the results obtained using the results from the French authors. The difference is clearly evident. The structural results obtained by Lavaud and Galy (1972) on CuV_2O_6 might suggest a phase transformation from the present structure to a monoclinic form.

A differential thermal analysis was run to find out such a transformation. Many runs were made using only the

Table 3-5

Empirical Bond Strengths in CuV_2O_6

Bond	French Authors				Present Result			
	Bond Length		Bond Strength		Bond Length		Bond Strength	
Cu-O(1)	1.92	2x	0.51	2x	1.904	2x	.542	2x
-O(2)	2.26	2x	0.22	2x	2.049	2x	.370	2x
-O(2)'	2.29	2x	0.20	2x	2.438	2x	.148	2x
			Σ=1.86				Σ=2.12	
V-O(1)b	2.57		0.16		2.588		0.155	
-O(3)a	2.08		0.47		2.056		0.501	
-O(1)a	1.70		1.30		1.697		1.310	
-O(2)a	1.63		1.78		1.655		1.494	
-O(3)d	1.97		0.61		1.871		0.799	
-O(3)d'	1.73		1.19		1.845		0.866	
			Σ=5.51				Σ=5.12	

sample mixed with the standard. We chose ammonium nitrate because this one has transitions in the regions we are looking for (T_{c_1} = 40°C, T_{c_2} = 94°C, T_{c_3} = 130°C). No evidence of such a transformation was found.

Table 3-6

Observed and Calculated Structure Factors for

CuV_2O_6

CHAPTER IV

$Ca_2V_2O_7$

EXPERIMENTS

The crystals of $Ca_2V_2O_7$ were prepared in accordance with a phase diagram of CaO and V_2O_5 given by J. J. Brown (38). Stoichiometric amounts of $CaCO_3$ and V_2O_5 were heated for several hours at 1380°C and allowed to cool slowly (6°C/hour) to 700°C at which temperature the platinum crucible was removed from the furnace and quenched. Microscopic examination of the sample showed that a fair number of single crystals were obtained. The crystals were yellow in color. One of these crystals was mounted on a precession camera. Precession photographs showed that the crystal was triclinic; no systematic absences were observed. From measurements of the d spacings, the approximate unit cell parameters were found to be

$a = 7.14$ Å $\quad b = 6.51$ Å $\quad c = 6.95$ Å

$\alpha = 94°$ $\quad \beta = 88°$ $\quad \gamma = 119°$

The crystal chosen for data collection had been ground in an air driven crystal grinder to an spherical shape such that its average diameter was 0.225 mm.

After the crystal was optically centered on the diffractometer ten reflections were chosen for centering. The unit cell parameters found by least squares refinement were:

$a = 7.240$ Å $\quad b = 6.663$ Å $\quad c = 6.913$ Å

$\alpha = 96.35°$ $\quad \beta = 87.68°$ $\quad \gamma = 119.55°$.

Calculated density = 3.529 g/cm^3

Measured density = 3.389 g/cm^3

The intensities were obtained from the above single crystal utilizing a Syntex $P\bar{1}$ automatic diffractometer (MoKα, graphite monochromatized, θ-2θ with variable scan rate, scintillation counter with pulse-height discrimination, a standard reflection measured at intervals of fifty reflections and backgrounds determined at 1° from either side of the peak). A total of 1334 reflections were measured with 1264 being observed. During the processing of the raw data, Lorentz and polarization corrections were applied.

The linear absorption coefficient μ_λ was calculated for molybdenum and chromium radiation for reasons outlined later, and found out to be $\mu_{Mo} = 54.82$ cm^{-1}, $\mu_{Cr} = 553.32$ cm^{-1}. The crystal was assumed to be spherical with an effective radius R=0.11 mm and hence $\mu_{Mo}R = 0.60$ and $\mu_{Cr}R = 6.08$. Absorption corrections were applied for the set of data taken with chromium radiation, but were not applied for the set taken with molybdenum radiation. The values of A*, the transmission factor, corresponding to the first set were obtained from the International Tables for X-ray Crystallography (36) and used to calculate the absorption correction factor for each reflection in the data set. The observed structure factors for the data

collected with molybdenum radiation are listed in Table 4-1.

A three dimensional Patterson function was calculated using all 1334 reflections of the data set collected with molybdenum radiation. A grid in steps of 1/22 along x, 1/17 along z and 1/20 along y was used. Inspection of the Patterson map showed many peaks which could be attributed to V-V interactions. In fact we have seen in Chapter 2 that the height of a given peak is proportional to the product of the atomic number associated with a given vector. In this case there are two calcium and two vanadium atoms in the asymmetric unit. These four atoms generate four single peaks, two vanadium and two calcium of the type (2x,2y,2z) and twelve double peaks which represent the possible combinations of the two calcium and two vanadium atoms $V_1 \pm V_2$, $Ca_1 \pm Ca_2$, $V_{1,2} \pm Ca_{1,2}$ of the type $(x_1 \pm x_2, y_1 \pm y_2, z_1 \pm z_2)$. However, the heights of these peaks can not clearly indicate which peaks correspond to the V-V interaction. This difficulty is probably a result of the fact that the atomic number of V and Ca are quite close and further, that two or three overlapping Ca-O or V-O interactions contribute as much as an interaction between a pair of the heavier scatterers. So the Patteron function was difficult to solve directly. Another method based on anomalous dispersion was developed to solve the Patterson function. This method will be described below together with the results applied in this structure.

It was shown in Chapter 3 that the normal scattering

Table 4-1

Observed Structure Factors for

$Ca_2V_2O_7$

(Data collected with molybdenum radiation)

factor must be corrected when the incident radiation falls near the natural absorption frequency of one of the scatterers. The correction consists of two terms, one real and one imaginary (see. eq. (2.36)). Thus the atomic scattering factor may show a significant difference if we choose two different radiations, one for which both the heavy atoms scatter normally (the corrections are negligible) and one for which an atom scatters anomalously (the corrections are important). Thus, the atomic scattering factor being different the corresponding atomic number Z will be different for the two radiations and consequently the heights of the peaks in the Patterson map will be different. In this manner the identification of the atomic contribution to the peaks in the Patterson can, in principle, be made. We will show now the above comments applied in our structure. The chromium and molybdenum radiations were chosen to try to distinguish between the two heavy atoms, Ca and V. The dispersion corrections for the atomic scattering factors for Ca and V are shown in Table 4-2. The values are taken from the International Tables for X-ray Crystallography (24).

Table 4-2

Dispersion Corrections for the Atomic Scattering Factor

	Mo radiation			Cr radiation	
	Δf'	Δf"		Δf'	Δf"
Ca	0.2	0.4	Ca	-0.2	2.7
V	0.3	0.7	V	-4.4	0.6

The meaning of Δf' and Δf" in the Table is the same as

in eq. (2.36). We can see that the corrections for molybdenum radiation are negligible. In the case of chromium radiation the corrections are important so we choose Z = 20 for Ca and Z = 19 for V. The imaginary corrections are not taken into account. For V they are essentially equal. The relative heights of the double peaks in the Patterson map are calculated using the above values for Z. The results are expressed in per cent relative to the origin peak. The value of the origin peak was calculated separately in both cases knowing that its weight can be expressed as follows:

$$\rho(ooo) = K \sum_{i=1}^{N} Z_i^2$$

where K is the proportionality constant needed to relate a peak from the absolute to the relative scale.

The results are presented in Table 4-3.

It is clear from this table that if we compare two Patterson maps, one collected using molybdenum and one using chromium radiation, the double V-V peak should decrease and the double Ca-Ca peak should increase while the Ca-V peak should remain unchanged.

Table 4-3

Relative Heights of the Double Peaks
Expressed in % of the Origin Peak

Mo radiation		Cr radiation	
Double peaks type	Heights %	Double peaks type	Heights %
V-V	23	V-V	18
Ca-Ca	17	Ca-Ca	20
Ca-V	20	Ca-V	19

Thus if we take the corresponding ratios of all the strong peaks from the two different Patterson maps, the double V-V peak should show an increased ratio and the double Ca-Ca peak should show a decreased ratio in comparison to the average ratio.

A second set of data collected with chromium radiation is needed to verify the above theory. The second set of data, using the same crystal, was collected using a film technique. The crystal was aligned along the b axis, and integrated Weissenberg photographs of the h0ℓ, h1ℓ, and h2ℓ planes were taken. To minimize the scaling problems, all the films were exposed for the same number of cycles and processed under the same conditions. The intensities were measured with a microdensitometer.

In order to obtain a scale which would include the intensities of both the strongest and the weakest reflections a number of reflections of medium intensity were measured with two different wedges on the optical densitometer. A scale factor was found which calibrated these wedges. Then those reflections which were measured using the strong wedge were rescaled using this scale factor. A total of 164 reflections were measured. In the processing of this raw data Lorentz and polarization corrections were applied along with correction for absorption. The relative structure factors from the three different layers, obtained in this manner still show a significant difference. To bring all the structure

factors to a common scale, the reflections from each layer were compared with the corresponding ones from the diffractometer data taken with molybdenum radiation. An average scale factor was found for each layer and each reflection was multiplied by the common scale factor. The observed structure factors for the data collected with chromium radiation are listed in Table 4-4. A three dimensional Patterson function was calculated using all the 164 reflections. The chromium Patterson was examined in layers perpendicular to the b axis. All the important peaks found in the molybdenum map were found in the chromium map, along with other spurious peaks. The chromium map contains a lot of spurious peaks and this is due to the fact that the number of reflections is too small and the Patterson series is assumed to be infinite (series termination effect). The main peaks in the chromium map are a little displaced in comparison to those in the molybdenum maps due to the same effect.

The results are presented in Table 4-5. The coordinates of fourteen peaks from both maps are listed. The relative peak heights expressed in per cent of the origin peak and the final ratio of equivalent peaks are also listed.

It can be seen be seen from this table that peaks 5, 9 and 12 show an increased ratio compared to the average, whereas peaks 2,3, 8 show a decreased one. Thus as discussed before the first peaks can be of V-V type and the second of Ca-Ca type.

Table 4-4

Observed Structure Factors for

$Ca_2V_2O_7$

(Data collected with chromium radiation)

Table 4-5

Comparison of the Relative Peaks Heights in the Patterson Function

	Mo radiation				Cr radiation				
Peak #	u	v	w	R^*_{Mo}	Peak #	u	v	w	R^*_{Cr}	$\frac{R_{Mo}}{R_{Cr}}$
1.	0.00000	0.00000	0.00000	100	1.	0.00000	0.00000	0.00000	100	1.00
2.	0.56818	0.02500	0.61764	9	2.	0.54545	0.00000	0.58823	12	0.75
3.	0.45454	0.04500	0.34117	9	3.	0.45454	0.02500	0.41176	12	0.75
4.	0.58863	0.04000	0.61176	12	4.	0.58863	0.05000	0.60000	13	0.92
5.	0.09545	0.05500	0.48823	23	5.	0.12727	0.05000	0.47058	14	1.64
6.	0.55454	0.10000	0.83529	18	6.	0.54545	0.05000	0.82352	14	1.28
7.	0.69090	0.14500	0.11176	9	7.	0.77272	0.15000	0.05882	7	1.28
8.	0.90909	0.30000	0.95294	7	8.	0.90909	0.30000	0.94117	7	0.77
9.	0.82272	0.35500	0.78235	14	9.	0.79545	0.40000	0.82352	8	1.75
10.	0.40909	0.40000	0.40588	13	10.	0.40909	0.45000	0.40000	13	1.00
11.	0.91818	0.40000	0.28823	26	11.	0.95454	0.45000	0.28235	27	0.96
12.	0.38181	0.47000	0.60588	16	12.	0.31818	0.45000	0.64705	8	2.00
13.	0.03636	0.50000	0.75882	22	13.	0.04545	0.50000	0.73529	26	0.84
14.	0.50454	0.45750	0.89705	24	14.	0.53636	0.50000	0.88235	19	1.26

where $R^* = \frac{P(u,v,w)}{P(o,o,o)}$

In the first attempted solution it was assumed that peaks 5 and 9 were the $V_1 \pm V_2$ type. With these two vanadium positions the calcium positions were calculated. The calculation was done by hand, knowing, as mentioned before, that the 10 strong peaks are of the $V_{1,2} \pm Ca_{1,2}$ type (double peaks). Most of the peaks were identified except peaks 3, 6 and 8. The attempt failed and we don't proceed further because it was clear from the beginning that the solution was wrong.

On the second attempt we assumed that peaks 5 and 12 were of the $V_1 \pm V_2$ type. The vanadium positions were found, and the calcium positions were calculated by hand, trying to identify all the peaks listed from the Patterson map. This time all the peaks were identified except number 10 which can be of the V-O type.

With these four atoms located two cycles of full matrix least squares refinement were run using the program CUDLS of X-ray 67 written by J. S. Stephens. The final positions for the four heavy atoms are listed below:

	x	y	z
V_1	.24251	.26370	.05339
V_2	.14915	.20591	-.44240
Ca_1	.68314	.15136	.22679
Ca_2	.82776	.30894	.67268

For this incomplete model an agreement factor of 0.43 was obtained. The bond distances between V_1 and V_2, and also between V_2 and Ca_2 are smaller, 2.59 Å and 2.79 Å, than normally

expected in these vanadate type structures (3.4-3.5 Å). For the sake of confidence we fit an oxygen atom between the two vanadium atoms and the agreement factor practically remained unchanged (R = 0.438). All these show that the solution is wrong again. In the last attempt we took another combination, peaks 5 and 14. They correspond to the V-V interaction according to the theoretical calculation (23 percent) and they both have the same height (as a sharpened Patterson map later run showed).

With these two positions found, a three-dimensional difference synthesis was calculated in order to locate the two calcium atoms. From the difference map , the two positions of the calcium atoms were clearly indicated. Again with these four heavy atoms located two cycles of full matrix least squares refinement were run. This time an agreement factor much lower was obtained R = 0.36. The bond distances between the two vanadium atoms seems reasonable but again the distance between one calcium and one vanadium seems to be too close V_1-Ca_2 = 2.81 Å.

The final positions of the four heavy atoms are listed below:

	x	y	z
V_1	.30603	.26583	.19617
V_2	.20740	.20032	.70128
Ca_1	.76480	.31303	.53350
Ca_2	.62155	.14612	.08718

Using these positional parameters for the four heavy atoms in the structure a three dimensional difference synthesis was calculated in order to locate the oxygen atoms. From the map the coordinates of two oxygen atoms were determined. With this incomplete model, after 2 cycles of least squares refinement, the agreement factor was 0.34. It was clear that the proposed solution was not the correct one. We try to fit again another oxygen in the structure, but no improvement was obtained. The R factor remained practically unchanged. The solution failed. From all these results it is clear that the structure is impossible to solve using only the information given by the direct Patterson function. The results given by the anomalous dispersion effect are also incomplete. The Patterson function constructed for chromium radiation contains too few reflections to be considered complete. More data are necessary and this can be done by trying to get upper layers along the same crystal axis or, something better using another axis. Another possibility will be to mount the same crystal on the diffractometer and collect the data in the same fashion using Cr radiation, Unfortunately this was not possible.

In another attempt to obtain the structure, use was made of the direct methods described in Chapter 2. The values of relative structure factors $|F_{rel\ hk\ell}|$ from the experimentally measured intensity (eq. (2.29)) are placed on an absolute scale using the program NORMSF of X-ray 71 (39). The program

calculates the normalized structure factors using eq. (2.56) and (2.58). In addition to that, statistical information needed in the direct phasing method is obtained. The program calculates statistical averages of normalized structure factors for centric and acentric distribution.

It has been recognized for a long time that for a crystal containing a reasonably large number of approximately equal atoms and at randomly distributed positions that the intensity distributions are different for centrosymmetric and non-centrosymmetric structure and also independent of structural complexity. Thus the values of statistical averages for the two different distributions can be used as a criterion in deciding if the space group is centrosymmetric or not. The experimental values together with theoretical values calculated for both cases are presented in Table 4-5.

Table 4-6

Normalized Structure Factors Statistical Averages

	Experimental	Theoretical	
		Centric	Acentric
$\langle\|E\|\rangle$	.815	.798	.886
$\langle\|E\|^2\rangle$	1.000	1.000	1.000
$\langle\|E^2-1\|\rangle$	.932	.968	.736
$\langle\|E^2-1\|^2\rangle$	1.548	2.000	1.000
$\langle\|E^2-1\|^3\rangle$	4.381	8.000	2.000

The statistical averages imply that the crystal is centrosymmetric and that the space group is $P\bar{1}$.

After the normalized structure factors have been obtained the Σ_2 relationships are calculated according to eq. (2.60) for all reflections with |E| values over a certain threshold. The program used for computation was SINGEN of X-ray 71 (39). The Σ_2 relations were computed from the 186 reflections with $|E| \geq 1.50$. The program listed all the triplets for each reflection, that is all the combinations of k and h-k for a given h. Along with each pair, k and h-k, the value of probability, eq. (2.61), that the product is positive is listed. The list is made for all reflections in order of decreasing magnitude of |E|.

The signs of three reflections are chosen so as to specify the origin. In making the phase assignments the largest suitable $|E_h|$ should be used. The choice will be determined by the extent to which a particular reflection enters into the combinations required by the Σ_2 relationships.

A set of three origin defining reflections was chosen on the basis of their high |E| values, their long Σ_2 listing and their interaction with each other. These were $(6,\bar{2},1)$, $(2,\bar{3},\bar{2})$ and $(3,1,\bar{1})$ whose signs were chosen to be +. Equation (2.60) was then employed to define as many signs of the largest $|E_h|$ as possible in terms of the specified ones and eq. (2.61) is used to calculate the corresponding probability of sign determination. When signs not longer can be assigned uniquely a symbol is assigned for the sign of a reflection, bearing in mind that the particular reflection should have a high number of triplets.

The phases of other reflections with large |E| values are calculated in this manner in terms of the specified signs and unknown symbols. The phase determination process is completed when the phases of all reflections of the chosen subset of all the whole set of reflections are determined.

We will briefly describe the mode of operation of the program PHASE (39) used in the phase determination which applies eq. (2.60). First the program calculates the phases of a small set of reflections in terms of specified signs and some symbolic phases which belong to the same set. (The symbolic phase is simply an integer that represents the rank of each reflection according to decreasing value of |E|). This subset of phases are called generators since once their signs are known many more phases can be determined without difficulty. After the generators are substituted into all Σ_2 the relationships and are used to generate all possible phases.

As we have mentioned before three reflections which define the origin were assigned positive signs. The first 35 symbolic phases were used as generators. On the first run of the program PHASE no other variables were assigned. From 35 generators, 10 phases are now defined in terms of the specified ones, 25 remaining unknown. From these, 21 are dependent in terms of two low symbolic phases. The probability as given by eq. (2.61) was set to 0.98 so that a phase should not be accepted if $P_+(h) \leq 0.98$. The generators applied to the whole set of

data gave only few additional phases.

In the next runs two more symbols were assigned reflections (5,0,5) and (5,2,5). In this manner all the generators, except one, are assigned a phase. Applied to the whole set of data 117 phases were thus defined (from the initial set of 186 phases).

In general if there are p unknown symbols assigned at most 2^p Fourier maps need to be computed. In actual practice there are many ways in which this number may be reduced. In our case the absence of a peak at the origin would eliminate a combination of values for the symbols for which the signs are predominantly plus. Likewise a predominantly negative set would also be unacceptable.

Three maps are calculated using E_h values whose signs have been determined. They are computed using 117 phases. This number of phases is obtained by taking the origin defining reflections with plus sign and the other two reflections with (5,0,5) and (5,2,5) plus or minus sign alternatively.

Thus the first map E_1 was computed assigning to the reflections (5,0,5) minus sign and to (5,2,5) plus sign, the second map E_2 assigning minus sign to both reflections and the third one changing the signs between the two reflections.

From all the three maps the positions of four atoms are clearly indicated. Having located these four atoms two cycles of full matrix least squares refinement were run using

the program CUDLS (X-ray 67 written by J. S. Stephens). The final positions of the four atoms are listed below in each case.

	E_1			E_2			E_3		
	x	y	z	x	y	z	x	y	z
V_1	.45918	.22024	.64319	.77781	.00743	.34753	.22202	.00723	.68225
V_2	.59077	.32209	.11447	.31765	.07286	.17422	.33258	.08968	.16018
Ca_1	.36623	.13319	.12619	.90714	.12209	.81909	.45969	.18559	.66446
Ca_2	.00897	.30572	.47207	.62260	.39247	.12744	.60338	.35763	.13748

All the three maps proved to be incorrect. The agreement factor R is oscillating between 0.53 and 0.62 for all three solutions, value which is much higher than normally expected.

The bond distances between vanadium and calcium atoms are smaller than normally expected in these vanadate type structure (3.4-3.5 Å). Thus for all three solutions the vanadium-calcium bond distance appears to be 1.5 Å.

The attempt failed and we didn't proceed further because it was clear that the proposed solutions were wrong. This was not unexpected as it is well known that direct methods are not very successful in the solution of triclinic structures.

GENERAL CONCLUSIONS

The structures of CuV_2O_6 and $Ca_2V_2O_7$ have been studied.

The structure of CuV_2O_6 has indicated that this metavanadate has a structure closely related to the mineral brannerite as do the majority of metavanadates. However, the symmetry of CuV_2O_6 appears to be reduced due to the Jahn-Teller distortion of CuO_6 octahedra.

Also, the present refinement of the parameters for CuV_2O_6 has indicated a bonding geometry consistent with other metavanadates. The structure has been tested for correctness using the bond strength-bond length relationship. The results obtained showed that the bond strength sum lies within 5% of the valence, which is consistent with the recent belief that for a well defined structure the discrepancies in bond strength sums should not exceed 5% of the valence.

The structure of $Ca_2V_2O_7$ will remain unsolved until a more complete data set can be obtained. The lack of sufficient data with chromium radiation places serious restrictions on the accuracy of the Patterson function. It is suggested that further work be undertaken using another crystal axis to have an adequate number of reflections. However, the unit cell parameters and the symmetry of the structure have been determined and possible solutions tried. The true solution can be obtained using this basis.

BIBLIOGRAPHY

1. R. Ruh and A. D. Wadsley, Acta Cryst. 21, 974 (1966).
2. J. C. Bouloux and J. Galy, Bull. Soc. Chim. Fr. 736 (1969).
3. G. Perez, B. Frit, J. C.Bouloux and J. Galy, C.R. Acad. Sci. Paris, C270, 952 (1970).
4. J. Angenault, Chim. Min. 7, 651 (1970).
5. H. N. Ng and C. Calvo, Can. Journal Chemistry 50, 3619 (1972).
6. S. Launay and J. Thoret, C. R. Acad. Sci., Ser. D 277, 541 (1973).
7. D. Lavaud and J. Galy, Bull. Soc. Fr. Miner. Cryst. 95, 134 (1972).
8. E. E. Sauerbrei , M.Sc. thesis, McMaster University, Hamilton, Ontario (1972).
9. C. Calvo and D. Manolescu, Acta Cryst. B29, 1743 (1973).
10. I. D. Brown and C. Calvo, J. Solid State Chem. 1, 173 (1970).
11. J. A. Baglio and J. N. Dann, G.T.E. Report (1970). Private communication.
12. R. Gopal and C. Calvo, Canadian Journal of Chemistry, 51 1004 (1973).
13. R. D. Shannon and C. Calvo, Canadian Journal of Chemistry 51, 70 (1973).
14. J. A. Baglio and J. N. Dann, J. Solid State Chem. 4, 98 (1972).
15. F. Hawthorne and C. Calvo. To be published.
16. J. Felsche, J. Less-Common Metals 21, 1 (1970).
17. C. Calvo, E. E. Sauerbrei and R. Faggiani (1974). To be published.

18. R. Gopal and C. Calvo. To be published in Acta Cryst.

19. E. Dorm and B. Marindor, Acta Chemica Scandinavica 21, 590 (1967).

20. P. K. Au and C. Calvo, Canadian Journal of Chemistry 45, 2297 (1967).

21. C. Calvo and R. Faggiani. To be published in Acta Cryst.

22. M. Quarton, J. Angenault and A. Rimsky, Acta Cryst. B29, 567 (1973).

23. W. H. Zachariasen, "Theory of x-ray diffraction in crystals" Dover Publications Inc., New York (1967).

24. International Tables for X-ray Crystallography, Vol. III, Kynoch Press, Birmingham (1952) p. 217.

25. A. L. Patterson, Z. Krist. A90, 517 (1935).

26. J. Karle and H. Hauptman, Acta Cryst. 3, 181 (1950).

27. J. Karle and I. L. Karle, Acta Cryst. 21, 849 (1966).

28. H. Hauptman and J. Karle, Acta Cryst. 6, 136 (1953).

29. E. N. Maslen, Acta Cryst. 22, 945 (1967).

30. G. H. Stout and L. H. Jonson "X-ray structure determination - a practical guide", McMillan, New York 1968), p. 306.

31. D. Sayre, Acta Cryst. 5, 60 (1952).

32. H. Hauptman and J. Karle. Solution of the Phase Problem. I. The Centrosymmetric Crystal. A.C.A. monograph No. 3, Pittsburgh Polycrystal Book Service (1953).

33. M. M. Woolfson. Acta Cryst. 7, 61 (1954).

34. P. Fleury, C.R. Acad. Sc. Paris 263, 1375 (1966).

35. X-ray Computing System, University of Maryland.

36. International Tables for X-ray Crystallography Vol. II, Kynoch Press, Birmingham (1952) p. 295.

37. I. D. Brown and R. D. Shannon, Acta Cryst. A29, 266 (1973).

38. J. J. Brown. Private communication.

39. J. M. Stewart, G. J. Krüger, F. A. Kundell and J. C. Baldwin, "X-ray system of October 1971", Computer Science Center, University of Maryland.